https://doi.org/10.5194/amt-2020-325
Preprint. Discussion started: 8 September 2020

Atmospheric Measurement Techniques Discussions

A comparison of three optical absorption photometers at a boreal forest site – effects of different correction algorithms

Krista Luoma[1], Aki Virkkula[2], Pasi Aalto[1], Katrianne Lehtipalo[1,2], Tuukka Petäjä[1] and Markku Kulmala[1]

[1]Institute for Atmospheric and Earth System Research, University of Helsinki, Helsinki, 00014, Finland
[2]Atmospheric Composition Research, Finnish Meteorological Institute, Helsinki, 00560, Finland

Correspondence to: Krista Luoma (krista.q.luoma@helsinki.fi)

Abstract.

We present a comparison between three absorption photometers that measured the absorption coefficient (σ_{abs}) of ambient aerosol particles in 2012 – 2017 at SMEAR II, a measurement station located in a boreal forest in southern Finland. The comparison included an Aethalometer (AE31), a Multi Angle Absorption Photometer (MAAP), and a Particle Soot Absorption Photometer (PSAP). These optical instruments measured particles collected on a filter, which is a source for systematic errors, since in addition to the particles, also the filter fibers interact with the radiation. To overcome this problem, several algorithms have been suggested to correct the data measured by the AE31 and the PSAP. Our aim is to study how the different correction algorithms affected the derived optical properties. We applied different correction algorithms to the AE31 and PSAP data, and compared the results against the reference measurements conducted by the MAAP. The comparison between the MAAP and AE31 resulted to a multiple scattering correction factor (C_{ref}) used in the AE31 correction algorithms to compensate for the scattering by the filter fibers. The C_{ref} varies between different environments, and our results are applicable for measurements conducted in a boreal environment. We observed a clear seasonal cycle of C_{ref}, which was probably due to the variations in aerosol optical properties, such as the backscatter fraction and single-scattering albedo, and also due to the variations in the relative humidity (*RH*) even though the *RH* in the instruments were kept below 40%. The results show that the filter measurement methods seem to be rather sensitive to the *RH* even if the *RH* is below the recommended value of 40%. The instruments correlated well ($R \approx 0.98$) but the slopes of the regression lines varied between the instruments and correction algorithms: compared to MAAP, the AE31 underestimated the σ_{abs} (the slopes varied between 0.93–0.97) and the PSAP overestimated the σ_{abs} (the slopes varied between 1.07–1.24). The instruments and correction algorithms had a notable influence on the absorption Ångström exponent: the median absorption Ångström exponent varied between 0.93 – 1.54 for the different algorithms and instruments.

https://doi.org/10.5194/amt-2020-325
Preprint. Discussion started: 8 September 2020

Atmospheric Measurement Techniques Discussions

1 Introduction

Atmospheric aerosol particles have a notable effect on the Earth's radiative balance. The particles affect the climate directly by scattering and absorbing the radiation from the sun, and indirectly through the aerosol-cloud interactions (Stocker et al., 2013). According to the IPCC report (Stocker et al., 2013), one of the greatest uncertainties in determining the global radiative forcing is related to atmospheric aerosol particles. Reasons for the large uncertainty are the complex nature of the aerosol-cloud interactions and also the large spatiotemporal variation of aerosol particles (Lohmann and Feichter, 2005). Since the number concentration, size distribution, chemical composition and the shape of the particles vary in both space and time, it is challenging to model and estimate the effect that the aerosol particles have on the climate in global scale (Stocker et al., 2013).

Generally, the direct effect of the particles on climate is cooling, since most of the particles scatter the light from the sun back in to the space (Stocker et al., 2013). However, if particles that are dark in color (i.e., highly absorbing) are located above a light colored surface (i.e., highly scattering), the particles have a warming effect on the climate. The sign of the aerosol forcing efficiency depends on the darkness of the particles, which is described by single scattering albedo, and on the albedo of the ground below the aerosol layer (Haywood and Shine, 1995). To determine the direct effect of the aerosol particles, in addition to the information about the albedo of the surface, we need measurements of aerosol optical properties (AOPs) like scattering, backscattering and absorption coefficient (σ_{sca}, σ_{bsca} and σ_{abs}). The σ_{sca} describes the ability of the particles to scatter the light in all directions, the σ_{bsca} describes the amount of scattering only in the backward direction and the σ_{abs} describes the ability of the particles to absorb light. All these variables are wavelength dependent, which is why the measurements are preferably conducted at multiple wavelengths

Measuring the σ_{sca} and σ_{bsca} of aerosol particles is rather straightforward and the measurements are typically conducted with an integrating nephelometer. The error sources and uncertainties of nephelometer measurements are well known (Anderson and Ogren, 1998; Müller et al., 2011b). However, for the σ_{abs} measurements there are still large uncertainties and the error sources are not as well defined as for the scattering measurements. The main difference between the σ_{sca} and σ_{abs} measurements is that the σ_{sca} measurement are conducted for particles suspended in air, whereas the σ_{abs} is typically measured by filter-based techniques, where the aerosol particles are first collected on a filter before the measurements. The problem with filter-based measurements is that in addition to the particles, also the filter fibers interact with the radiation, which influences the measurements.

One of the issues with the optical filter measurements is the multiple scattering of light by the filter fibers. The scattering by the filter fibers is taken into account by the so-called multiple scattering correction factor (C_{ref}). Even though the C_{ref} should only depend on the filter properties, previous studies have shown that the C_{ref} depends also on the particulate matter suspended in the filter (Arnott et al., 2005; Collaud Coen et al., 2010; Weingartner et al., 2003). The C_{ref} has been observed to vary from

https://doi.org/10.5194/amt-2020-325
Preprint. Discussion started: 8 September 2020


Atmospheric Measurement Techniques Discussions

station to station and therefore it has been studied in different types of environments. For example, Collaud Coen et al. (2010) studied the C_{ref} at very clean mountain sites, in a maritime site, and in more urban areas; Schmid et al. (2006) did observations in Amazonia; Backman et al. (2017) studied the C_{ref} in Arctic sites; and Kim et al. (2019) ran measurements in a maritime, high altitude, and Arctic sites. In our study, one of the aims is to provide a C_{ref} value suitable for a boreal forest site and to study how the C_{ref} varies between different correction algorithms.

Another issue with the optical filter measurements is related to the nonlinear response of the instruments as the filter is loaded with particles. When the filter is loaded with absorbing particles, the particles cast a so-called shadowing effect, which decreases the response of the instrument. Therefore, the instruments report a lower σ_{abs} for loaded filters compared to pristine filter measurements. Several studies have developed algorithms and determined coefficients to overcome this problem observed with different instruments (Arnott et al., 2005; Bond et al., 1999; Collaud Coen et al., 2010; Li et al., 2020; Müller et al., 2014; Ogren, 2010; Schmid et al., 2006; Weingartner et al., 2003; Virkkula et al., 2005; Virkkula et al., 2007; Virkkula, 2010). The outcome of the different algorithms, however, varies and they may affect for example the wavelength dependency of the σ_{abs}. Another aim of this study is to present how the different correction algorithms of the σ_{abs} affect the measured optical properties of the particles.

The measurements presented in this study, were conducted in 2012 – 2017 at the SMEAR II (Station for Measuring Ecosystem-Atmosphere Relations II; Hari and Kulmala, 2005), which is located in the middle of a boreal forest in southern Finland. During this period, the AOPs at SMEAR II have been measured by several instruments: an integrating nephelometer and three different absorption photometers (AE31, PSAP, and MAAP), which enabled determining the C_{ref} and an extensive comparison between the different instruments and correction algorithms. AOPs at SMEAR II have been extensively discussed by Virkkula et al. (2011) and Luoma et al. (2019), however, these studies focused on the temporal variation of the AOPs and they only discussed nephelometer and AE31 data. In this study, we focus on the technical side of the measurements and instrument comparison.

2 Measurements and methods

2.1 The field site

The measurements took place at the SMEAR II station (Station for Measuring Ecosystem-Atmosphere Relations; Hari and Kulmala, 2005). The measurement station locates in Hyytiälä, Southern Finland (61°51'N, 24°17 E). SMEAR II is a rural measurement station and it represents boreal forest environment. The area around the station is mostly forests, which consists mainly of scots pine trees (Hari et al., 2013). The site is classified as rural and there are no remarkable sources of pollution nearby. The area is sparsely populated; are few smaller towns and some scattered settlements. The closest bigger cities are Tampere (220 000 inhabitants) and Jyväskylä (140 000 inhabitants) and they are located 60 and 100 km away from the station.

https://doi.org/10.5194/amt-2020-325
Preprint. Discussion started: 8 September 2020


Atmospheric Measurement Techniques Discussions

2.2 Instrument set-up

The measurements of AOPs for PM10 particles were started already on June 2006 with an integrating nephelometer (TSI model 3563) and an Aethalometer (Magee Scientific model AE31). Later on there has also been a Particle Soot Absorption Photometer (PSAP; Radiance Research model 3-λ; Virkkula et al., 2005), a Multi-Angle Absorption Photometer (MAAP; Thermo model 5012; Petzold and Schönlinner, 2004) and a Cavity Attenuated Phase Shift extinction monitor (CAPS, Aerodyne Research; Kebabian et al., 2007) . The CAPS was deployed at the SMEAR II to measure the extinction coefficient (σ_{ext}) of airborne particles. However, the CAPS data was invalidated from this study due to technical issues and therefore the instrument is not discussed in this article. Even though the AOP measurements have been conducted at SMEAR II already since 2006, in this study we consider only data measured after January 2012 until December 2017. This period was selected to have all the three absorption instruments running in parallel: the AE31 stopped operating in December 2017, the PSAP operated from January 2012 to March 2016, and the MAAP started operation in June 2013. Also, during this period there were only few changes in the measurement line: in March 2017 the MAAP flow was decreased from 18 lpm to 9 lpm and Nafion dryers were installed in front of MAAP; and in November 2017 one of the two Nafion dryers were removed in front of the Nephelometer.

The instruments measured AOPs at different wavelengths: the integrating nephelometer measured the σ_{sca} and σ_{bsca} at three wavelengths (450, 550 and 700 nm); the AE31, the PSAP and the MAAP measured the σ_{abs} at seven (370, 470, 520, 590, 660, 880 and 950 nm), three (467, 530 and 660 nm), and one wavelength (637 nm), respectively.

The data availability of all the optical data for the studied period sets are reported in Fig. 1. Some of the data were missing or invalidated due to instrument malfunctions, too high relative humidity (*RH*), too loaded filter, or due to the absence of the instrument because of workshops or campaigns. If the *RH* exceeded 40% in an instrument, the data was marked as invalid. Before the dryers were installed for the MAAP in March 2017, some of the MAAP data, especially from the summer, had to be invalidated due to too high humidity. During the cold season, the indoor temperature at the measurement cottage was higher than outdoors and therefore the *RH* decreased when the sample air was warmed up to the indoor temperature (passive drying). However, during the summer the *RH* sometimes increased above accepted limit since the passive drying was not enough due to minimal difference between the indoor and outdoor temperature.

The measurement arrangement of the instruments, which measured AOPs, is presented in Fig 2. The schematic figure represents the measurement line from that time when all the instruments mentioned before were measuring in parallel, which was during 2014 – 2015. In the beginning of the measurement line, a pre-impactor removed all the particles that were larger than 10 µm in aerodynamic diameter from the sample air (i.e., PM10 particles passed the pre-impactor). The air flow trough

https://doi.org/10.5194/amt-2020-325
Preprint. Discussion started: 8 September 2020


Atmospheric Measurement Techniques Discussions

another impactor, which removed all the particles larger than 1 µm (i.e., PM1 particles passed the impactor) was controlled by two valves. The valves changed the direction of the flow in every 10 minutes, so that in a 20 minutes measurement cycle the instruments measured 10 minutes of the PM10 particles and then 10 minutes of the PM1 particles. The sample air was dried with Nafion dryers for the PSAP, AE31 and integrating nephelometer for the whole period and for the MAAP since March 2017.

2.3 Absorption measurements

As mentioned above, the σ_{abs} of aerosol particles at different wavelengths at SMEAR II was measured with three different instruments: AE31, PSAP and MAAP. Each of these instruments measure the σ_{abs} by filter-based technique, which means that the measurements are conducted for aerosol particles that are collected on a filter.

The AE31 and the PSAP have a similar measurement principle (Bond et al., 1999). Before the σ_{abs} can be determined by using different correction algorithms, the instruments measure the attenuation coefficient (σ_{ATN}), which describes the attenuation of light through the sample collected on the quartz fiber filter. The equation for the σ_{ATN} is derived from the Beer-Lambert-Bouguer law

$$\boldsymbol{\sigma_{ATN}} = \frac{\boldsymbol{A}}{\boldsymbol{Q\,\Delta t}} \ln\frac{\boldsymbol{I_{t-\Delta t}}}{\boldsymbol{I_t}} = \frac{\boldsymbol{A}}{\boldsymbol{Q}}\frac{\boldsymbol{\Delta ATN}}{\boldsymbol{\Delta t}}, \quad (1)$$

where A is the sample area on the filter, Q is the flow through the filter, and t is the time. $I_{t-\Delta t}$ and I_t are the measured light intensities through the filter in the beginning of the measurement period ($t - \Delta t$) and in the end of the measurement period (t) and ΔATN is the change in attenuation (ATN), which is calculated from the ratio of light intensity through a clean filter (I_0) and through a loaded filter (I_t) as

$$ATN = -\ln\left(\frac{I_t}{I_0}\right) \cdot 100\% . \quad (2)$$

In addition to the ATN, the filter loading can also be described by transmittance (Tr)

$$Tr = I_t I_0^{-1}, \quad (3)$$

which can be also presented as a function of ATN (Tr = exp(ATN/100%)). The ATN and Tr represent essentially the same concept, but the way of expressing the change of intensity depends on the instrument used: the ATN is traditionally associated with Aethalometer data and Tr with PSAP data.

In Eq. 1, A is typically a constant value defined by the manufacturer and Q is recorded and reported by the instrument. These values, however, might deviate notably from the real values, and therefore they should be measured. A should be checked regularly and Q should be monitored continuously and calibrated regularly with a calibrated flow meter. If these values differ from the reported ones, the Eq. 1 needs corrections for the A and the Q.

https://doi.org/10.5194/amt-2020-325
Preprint. Discussion started: 8 September 2020


Atmospheric Measurement Techniques Discussions

In the filter, the light is attenuated because of the absorption and scattering by the particles, but also because of the scattering by the filter fibers, which is called multiple scattering. The scattering by the filter fibers increase the optical path of the light beam through the filter. Therefore, the probability for the light beam to be absorbed by a particle increases. Because of the scattering in the filter medium, the σ_{ATN} is larger than the σ_{abs}. Not only the filter fibers scatter light, but also the embedded aerosol particles scatter light affecting the absorption measurements, causing the so-called apparent absorption, which is typically taken into account by subtracting a fraction of scattering from the σ_{ATN}. As the filter gets more loaded with particles, the response of the instrument gradually changes. Absorbing particles induce a so-called "shadowing effect", introduced by Weingartner et al. (2003), decreases the change in the intensity ($I_{t-\Delta t} I_t^{-1}$) as the filter gets more loaded. This means that the response of the instruments is not linear for different filter loadings. The increasing filter loading has an opposite effect than the scattering of the filter fibers and particles: the absorbing particles collected on the filter decrease the optical path and therefore the reported σ_{ATN} for a loaded filter is lower than for a pristine filter. This non-linearity is taken into account in the various correction algorithms presented in Sect. 2.3.1 and 2.3.2.

The measurement principle of the MAAP is different from the AE31 and PSAP (Petzold and Schönlinner, 2004). In addition to the light attenuation measurements, the MAAP also measures the backscattered light from the filter in two different angles. The σ_{abs} is then obtained by using a radiative transfer scheme where the measurements of the backscattering and light attenuation are taken into account (Petzold and Schönlinner, 2004). Because of the backscattering measurements, the MAAP does not suffer as much from the filter artefacts as the Aethalometer and the PSAP and hence it does not need any correction algorithms. However, in very polluted environments also the MAAP suffers from a measurement artifact that has to be corrected (Hyvärinen et al., 2013), which at SMEAR II, however, is not the case.

The reported uncertainties of the MAAP, PSAP and Aethalometer are respectively 12, 13, and as large as 50 % (Arnott et al., 2005; Ogren, 2010; Petzold and Schönlinner, 2004). Müller et al. (2011a) reported that the unit-to-unit variability of the PSAP, Aethalometer and MAAP were about 8%, 20% and 3%. Since the uncertainty and unit-to-unit variability of the MAAP was a lot smaller than for the PSAP and Aethalometer and because the measurement principle of the MAAP is independent from the PSAP and AE31, since it uses the radiative transfer scheme, we used the MAAP as the reference instrument for measuring σ_{abs}.

Each of the absorption instrument used in this study have their strengths and weaknesses that determine which instrument is the most useful in different situations. According to the uncertainty and unit-to-unit variability, the MAAP is the most accurate instrument for monitoring σ_{abs} and black carbon (BC) concentration, which is typically derived from σ_{abs} measurements. The MAAP changes the spot in a filter roll automatically and therefore it does not require much assistance from the operator and the instrument can run at a remote station as well. However, it measures the σ_{abs} only at one wavelength so it is not possible to do the source apportionment or interpretation on the chemical composition of the absorbing particles, which requires

https://doi.org/10.5194/amt-2020-325
Preprint. Discussion started: 8 September 2020


Atmospheric Measurement Techniques Discussions

measurements on several wavelengths (see Sect. 3.1 and Eq. 16). The AE31 again has a very wide range of wavelengths, which makes the seven-wavelength Aethalometers, the AE31 and the new model AE33, functional and popular instruments. Like MAAP, the AE31 also operates the filter roll automatically so the instrument does not need that much assistance from the operator. Unfortunately, the problems with defining the errors caused by the filter material are not that well defined, and the instrument uncertainty and unit-to-unit variability is large. The uncertainty and noise of the PSAP is smaller than that of the AE31, which makes the PSAP a popular especially in areas with low concentrations. Even though the wavelength range is not as good as with AE31, the PSAP measures the σ_{abs} at three wavelengths, allowing the use of applications that need the wavelength dependency of σ_{abs}. The problem with PSAP is that the filter has to be changed manually by the user so the instrument is not the best option to deploy at a remote site.

2.3.1 AE31 correction algorithms

To determine the σ_{abs} from AE31 measurements, the σ_{ATN} needs to be corrected for the multiple scattering by the filter fibers and for the error caused by the filter loading, and in addition, the scattering of aerosol particles should also be taken into account

$$\boldsymbol{\sigma_{abs}} = \frac{\boldsymbol{\sigma_{ATN} - a_s\,\sigma_{sca}}}{\boldsymbol{C_{ref}\,R(ATN)}}. \quad (4)$$

The effect of the multiple scattering is corrected with a multiple scattering correction factor (C_{ref}) and it is larger than unity. For the filter loading correction ($R(ATN)$) there are different kind of correction algorithms developed for example by Weingartner et al. (2003), Arnott et al. (2005), Schmid et al. (2006), Virkkula et al. (2007), and Collaud Coen et al. (2010). The R, which equals unity for unloaded filters is less than unity for loaded filters, depends on the filter loading, i.e., ATN defined in Eq. (2).

In Eq. (4), the scattering by the aerosol particles is taken into account by subtracting a fraction (a_s) of the measured scattering (σ_{sca}). However, the algorithms by Weingartner et al. (2003) and Virkkula et al. (2007) ignore the particle scattering subtraction, which makes it possible to apply the corrections algorithms without any σ_{sca} measurements. In Weingartner's algorithm, however, σ_{sca} is taken into account without the subtraction, as will be shown below. For a comparison, in this study we also present data, which was corrected only for the multiple scattering and not for the filter loading (i.e., the R = 1) or scattering by the particles. Below we present the different algorithms determined by Weingartner et al. (2003), Arnott et al. (2005), Virkkula et al. (2007), and Collaud Coen et al. (2010), which were selected to use in this study.

Current recommendation by the WMO and GAW is to assume the $R(ATN)$ unity for the AE31 and to use a C_{ref} value of 3.5, which was determined by a comparison study of different AE31 instruments (WMO/GAW, 2016). Therefore, we also studied

https://doi.org/10.5194/amt-2020-325
Preprint. Discussion started: 8 September 2020


Atmospheric Measurement Techniques Discussions

"not-corrected" AE31 data for which we did not apply any *R(ATN)* correction or particulate scattering reduction, but only the multiple scattering correction.

Weingartner et al. (2003) derived an empirical correction algorithm based on laboratory measurements of mixed particles (soot, diesel exhaust, organic coating, ammonium sulfate). Hereon we refer to the algorithm as W2003 and with the subscript WEI. The W2003 correction algorithm interpolates the measurements at higher *ATN* values, to a point where *ATN* was 10%. When *ATN* is lower than 10%, the *R* is assumed unity. In W2003 the loading correction R_{WEI} is

$$R_{\mathrm{WEI}}(ATN) = \left(\frac{1}{f} - 1\right)\frac{\ln(ATN) - \ln(10\%)}{\ln(50\%) - \ln(10\%)} + 1. \quad (5)$$

Weingartner et al. (2003) stated that the *R* is ω-dependent and they found the following relation for the factor *f*

$$f = a(1 - \omega) + 1. \quad (6)$$

In Eq. 6, the *f* is unity (i.e., *R* is unity), when the ω is unity (i.e., the aerosol is purely scattering). Weingartner et al. (2003) determined that the *a* in Eq. 6 was 0.87 and 0.85 at 450 and 660 nm, respectively. According to these values, we interpolated the *a* for all the seven wavelengths by assuming a linear wavelength dependency. Also, the ω was interpolated to the seven AE31 wavelengths according to the mean σ_{abs}, σ_{sca} and α_{sca} values reported by Luoma et al. (2019; see their article Table 1) for PM10 particles. Using these values, we estimated the *f* separately for each wavelength and we used those constant values in the correction values. The resulted *a*, ω, and *f* were slightly wavelength dependent and their values are presented in Table 1.

The correction algorithm does not apply the scattering correction by subtraction, so the $a_{\mathrm{s,WEI}}$ = 0 and therefore parallel scattering measurements are in principle not needed. However, the effect of the particulate scattering is taken into account in the *f* since it depends on the ω. If there are no parallel measurements of σ_{sca}, the ω cannot be determined. If there is no estimation on the ω, typically *f* values for different aerosol types determined by Weingartner et al. (2003) are used. The *f* values were close to the result Weingartner et al. (2003) acquired from measurements of ambient aerosols in a high alpine site and in a garage (*f* was 1.03 and 1.14 for a "white light" Aethalometer; AE10). For example, Collaud Coen et al. (2010) estimated an intermediate value *f* = 1.10 for Cabauw measurements site based on the study by Weingartner et al. (2003).

Arnott et al. (2005) suggested a correction algorithm, which is hereon we referred as A2005 and with the subscript ARN, based on a well-defined theoretical basis. One big difference to the W2003 is that there is a factor for scattering subtraction. Arnott et al. (2005) determined the scattering subtraction fraction $a_{\mathrm{s,ARN}}$ from laboratory measurements using submicron ammonium sulfate particles and the values for different wavelengths are presented in Table 1, however, Arnott et al. (2005) noted that the values of $a_{\mathrm{s,ARN}}$ could be different if supermicron aerosol particles are present. The loading correction R_{ARN} was defined as:

$$R_{\mathrm{ARN}}(ATN) = \left(\sqrt{1 + \frac{\left(\frac{V\Delta t}{A}\right)\sum_{i=1}^{n-1}\sigma_{\mathrm{abs},i}}{\tau_{a,fx}(\lambda)}}\right)^{-1}, \quad (7)$$

https://doi.org/10.5194/amt-2020-325
Preprint. Discussion started: 8 September 2020


Atmospheric Measurement Techniques Discussions

where the n indicates the n^{th} measurement after a filter spot change. The correction takes in to account the cumulative σ_{abs} of the particles collected on the filter material. The $\tau_{a,fx}(\lambda)$ is the filter absorption optical depth for the filter fraction x that has particles embedded. The used $\tau_{a,fx}$ values are presented in Table 1 and they were calculated from a power law function $\tau_{a,fx}(\lambda) = \tau_{a,fx,521} \cdot (\lambda/521\ \text{nm})^{-0.754} = 0.2338 \cdot (\lambda/521\ \text{nm})^{-0.754}$. The exponent -0.754 was obtained from a power function fitting to $\tau_{a,fx}$ vs. λ (Table 1 of Arnott et al., 2005), similar as in Virkkula et al. (2011). The $\tau_{a,fx,521} = 0.2338$ is the recommended $\tau_{a,fx}$ value for ambient measurements at 521 nm (Arnott et al., 2005).

Virkkula et al. (2007) proposed a correction algorithm, which is hereon referred as V2007 and with the subscript VIR, that utilizes the so-called compensation parameter (k). The k is determined by comparing the last measurements of a loaded filter to the first measurements conducted with a pristine filter. The compensation parameter is determined for each filter spot (fs) as follows:

$$k_{fs} = \frac{\sigma_{\mathrm{ATN}}(t_{fs+1,\mathrm{first}}) - \sigma_{\mathrm{ATN}}(t_{fs,\mathrm{last}})}{ATN(t_{fs,\mathrm{last}})\sigma_{\mathrm{ATN}}(t_{fs,\mathrm{last}}) - ATN(t_{fs+1,\mathrm{first}})\sigma_{\mathrm{ATN}}(t_{fs+1,\mathrm{first}})}, \quad (8)$$

where the "first" refers to the mean of three first values in a pristine filter (i.e., $fs + 1$) and the "last" refers to the mean of three last values in a loaded filter (i.e., fs). The k is then applied in the loading correction R_{VIR}

$$R_{\mathrm{VIR}}(ATN) = \left(1 + k_{fs} ATN\right)^{-1}. \quad (9)$$

This algorithm does not take into account the scattering correction so the $a_{s,\mathrm{VIR}} = 0$.

Collaud Coen et al. (2010) applied this correction to data from several stations in Europe and found that it was highly nonstable and that it leads to large outliers. They correctly stated that the difficulty of applying this correction is due to the natural high variability of σ_{ATN} as a function of time, which is for most of the time greater than the σ_{ATN} decrease induced by filter changes. We therefore calculated the running average compensation parameter for all seven wavelengths in order to minimize these problems. Then we applied this averaged compensation parameter to correct the non-corrected AE31 data. In other words, the AE31 data were not averaged at this stage, just the compensation parameter.

We determined the k as a 14-day running mean (±7 days around the changing time of the filter spot), since without the averaging the k was very noisy (see time series for the non-averaged and averaged k in Fig. S3). Averaging the k was also recommended by Virkkula et al. (2007). On average, the 14-day-periods included about nine data points (i.e., the filter spot changed on average about once a day). Virkkula et al. (2015) used a similar approach for AE31 data from Nanjing, China, and calculated 24-hour running averages of the k including on the average six filter spot changes.

Collaud Coen et al. (2010), which is hereon referred as CC2010 and with the subscript COL, correction algorithm was based on the W2003 algorithm but here the reference ATN for the clean filter is 0 % instead of 10 %. They determined the a used in

https://doi.org/10.5194/amt-2020-325
Preprint. Discussion started: 8 September 2020


Atmospheric Measurement Techniques Discussions

Eq. 6 a bit differently and got a mean value of a = 0.74 over different wavelengths and different experiments. The R_{COL} is defined as

$$R_{\mathrm{COL}}(ATN) = \left(\frac{1}{a(1-\bar{\omega}_{0,n})+1} - 1\right) \cdot \frac{ATN}{50\%} + 1. \quad (10)$$

Here the $\bar{\omega}_{0,fs,n}$ stands for the mean $\bar{\omega}_0$, that was calculated for the filter spot from the first measurements to the n^{th} measurement. The $\bar{\omega}_{0,fs,n}$ was determined by using the σ_{ATN} as the first estimate of the σ_{abs}. CC2010 differs from the W2003 also by taking into account the scattering correction. They suggested two different kind of ways to determine $a_{\mathrm{s,COL}}$ and here we present the one that was determined in a manner similar to A2005. The difference to the $a_{\mathrm{s,ARN}}$ is that the $a_{\mathrm{s,COL}}$ is determined from the ambient scattering measurements so it is not constant. The $a_{\mathrm{s,COL}}$ is defined similarly as by Arnott et al. (2003) (Eq. 8 in their article), but here they used measured scattering properties instead of constant values determined by laboratory measurements:

$$a_{\mathrm{s,COL}} = \bar{\beta}_{\mathrm{sca},n}^{d-1} c \lambda^{-\bar{\alpha}_{\mathrm{sca},n}(d-1)}, \quad (11)$$

where d = 0.564 and c = 0.329 · 10^{-3}. In Eq. 11 the over lined variables, $\alpha_{\mathrm{sca,n}}$ and $\beta_{\mathrm{sca,n}}$, stand for average properties of aerosols deposited in the filter i.e., mean values from the beginning of the filter measurements until the n^{th} measurement. The $\alpha_{\mathrm{sca,n}}$ is the scattering Ångström exponent (see Sect. 3.1 and Eq. 16) and the β_{sca} is acquired from the power-law fit of the wavelength dependency of σ_{sca}:

$$\sigma_{\mathrm{sca}} = \beta_{\mathrm{sca}} \lambda^{-\alpha_{\mathrm{sca}}}, \quad (12)$$

where the fit is calculated with λ and σ_{sca} in units nm and Mm^{-1} to acquire unitless β.

2.3.2 PSAP correction algorithms

Since the measurement principles of PSAP and AE31 are basically the same, the PSAP data needs similar kind of corrections as the AE31 data (Eq. 2). In this study the PSAP data was corrected with two algorithms: one described by Bond et al. (1999) and later specified by Ogren (2010), which is hereon referred as the B1999; the other determined by Virkkula et al. (2005) and later corrected by Virkkula (2010), which is hereon referred as the V2010. The algorithms of Müller et al. (2014) and Li et al. (2020) were not applied.

The B1999 correction algorithm is given by

$$\sigma_{\mathrm{abs}} = 0.85 \frac{\sigma_{\mathrm{PSAP}}}{K_2} - \frac{K_1 \sigma_{\mathrm{sca}}}{K_2}, \quad (13)$$

where the K_1 = 0.02 and K_2 = 1.22 and

$$\sigma_{\mathrm{PSAP}} = \frac{\sigma_{ATN}}{1.0796 \cdot Tr + 0.71}. \quad (14)$$

In the V2010 correction algorithm, the σ_{PSAP} is determined in an iterative manner. The first estimation of absorption coefficient ($\sigma_{\mathrm{abs,0}}$), which is determined by $\sigma_{\mathrm{abs,0}} = (k_0 + k_1 \ln(Tr))\sigma_{ATN} - s\sigma_{\mathrm{sca}}$, where the k_0 and k_1 are constants presented in Table 1

https://doi.org/10.5194/amt-2020-325
Preprint. Discussion started: 8 September 2020


Atmospheric Measurement Techniques Discussions

in Virkkula (2010). The $\sigma_{abs,0}$ is used to calculate the single scattering albedo ω (see Sect. 3.1 and Eq. 17), which is then again used to calculate the σ_{abs} again in an iterative manner, but now with a different kind of an equation

$$\sigma_{\mathrm{abs}} = (k_0 + k_1 h(\omega_0) \ln(Tr))\sigma_{ATN} - s\sigma_{\mathrm{sca}}, \quad (15)$$

where the $h(\omega_0) = h_0 + h_1\omega$. The ω is then calculated again with Eq. 17. These two steps are repeated until the change in the σ_{abs} is minor. We agreed the result, when the change was less than 1%. It must be noted that this correction algorithm is different from the V2007 determined for the Aethalometer data.

2.4 Scattering measurements

The σ_{sca} data is needed in order to subtract a fraction of particulate scattering from the σ_{ATN} in A2005, CC2010, B1999 and V2010. Measurements of σ_{sca} and σ_{bsca} are also needed in determining the ω and the backscatter fraction (b, see Sect. 3.1 and Eq. 18), which are used to explain the observed variations in the results. The ω is also used in CC2010.

The σ_{sca} and σ_{bsca} were measured with an integrating nephelometer (TSI model 3565, Anderson et al., 1996) . The integrating nephelometer measured σ_{sca} and σ_{bsca} at three wavelengths (450, 550 and 700 nm). Due to instrumental restrictions, the nephelometer can only measure σ_{sca} on the range of 7° – 170° and σ_{bsca} on the range of 90° – 170°, and therefore a truncation correction is applied to σ_{sca} and σ_{bsca} measurements (Anderson and Ogren, 1998; Bond et al., 2009). The uncertainty of the integrating nephelometer has been reported to be below ± 10 % (Anderson et al., 1996).

3 Data analysis

All the data were averaged for 1 h intervals. The PM1 and PM10 measurements were not separated in the data analysis, but instead both PM1 and PM10 data were averaged together. Since the instrument measured in the same size range, mixing the PM1 and PM10 data cause no difference between the instruments.

3.1 Intensive properties

The intensive properties of aerosol particles are determined from the measurements of the extensive properties, which in our data are σ_{abs}, σ_{sca}, and σ_{bsca}. In addition to the chemical properties and size distribution, the extensive properties also depend on the number and volume concentration of the particles. The intensive properties, however, are independent of the amount of the particles and they depend only on the properties of the particles, such as the shape of the size distribution, chemical composition and shape of the particles. Therefore, intensive properties are useful parameters as they indirectly indicate the properties of the particle population. The intensive properties used in this article are the Ångström exponent (α), single scattering albedo (ω), and backscatter fraction (b) and they are presented below.

https://doi.org/10.5194/amt-2020-325
Preprint. Discussion started: 8 September 2020


Atmospheric Measurement Techniques Discussions

The Ångström exponent, (α) describes the wavelength dependency of the optical properties and it can be calculated for example for σ_{abs} and σ_{sca} to acquire the absorption Ångström exponent (α_{abs}) and scattering Ångström exponent (α_{sca}), respectively. The α is defined by

$$\alpha = -\frac{\ln\frac{\sigma_1}{\sigma_2}}{\ln\frac{\lambda_1}{\lambda_2}}, \quad (16)$$

where the σ_1 and σ_2 are the property for which the α is being calculated at wavelengths λ_1 and λ_2, respectively. The α is typically used to interpolate or extrapolate optical properties to different wavelengths. This is useful for example in cases, when instruments measure optical properties at different wavelengths and the measurements between different instruments need to be compared. The wavelength dependency also gives information about the size distribution, chemical composition, and sources of the particles: α_{sca} depends on the size distribution of the particles and α_{abs} depends on both the chemical composition and size distribution. The α_{abs} is typically used in source apportionment models of black carbon (BC) (Sandradewi et al., 2008; Zotter et al., 2017).

One commonly used property is the single-scattering albedo (ω), which describes how big fraction of the total light extinction ($\sigma_{abs} + \sigma_{sca}$) is due to scattering:

$$\omega = \frac{\sigma_{sca}}{\sigma_{sca}+\sigma_{abs}}. \quad (17)$$

The lower ω is, the darker the aerosol particles are, which is typically caused by a higher content of black carbon (BC); ω close to unity indicates that the particles are high in scattering material like sulfates or sea salt. Therefore, ω is a rough indicator of the chemical composition of the particles.

The backscatter fraction (b) describes the fraction of backscattering coefficient (σ_{bsca}; meaning that the light scatters in the backward hemisphere) of the total scattering coefficient (σ_{sca}):

$$b = \frac{\sigma_{bsca}}{\sigma_{sca}}. \quad (18)$$

The b is also size dependent. In molecular size range it is 0.5, which means that the particles scatter light evenly in the forward and in the backward direction. For larger particles the b decreases, so the particles scatter light more in the forward direction. Compared to α_{sca} the b is less sensitive to bigger particles.

3.2 Multiple scattering correction factor

As stated by Weingartner et al. (2003), the C_{ref} should in principle only depend on the instrument and the filter material used. The effect caused by different amount of particles deposited in the filter material and their optical properties should be taken into account by the empirical filter loading correction functions $R(ATN)$. However, as shown by previous studies, the C_{ref} varies

https://doi.org/10.5194/amt-2020-325
Preprint. Discussion started: 8 September 2020


Atmospheric Measurement Techniques Discussions

both spatially and temporally (Backman et al., 2017; Collaud Coen et al., 2010) and therefore we determined the C_{ref} also at SMEAR II.

In this study, the multiple scattering correction factor (C_{ref}) was defined for the AE31 measurements by using the σ_{abs} measured by the MAAP as the reference absorption coefficient ($\sigma_{abs,ref}$). To determine the C_{ref}, the σ_{ATN} measured by the AE31 had to be corrected for the artefact caused by the increased filter loading and then the measurements can be compared to the reference absorption ($\sigma_{abs,ref}$) measured by the MAAP

$$\boldsymbol{C_{ref}} = \frac{\boldsymbol{\sigma_{ATN}}}{\boldsymbol{R(ATN)\,\sigma_{abs,ref}}}. \quad (19)$$

The C_{ref} was defined separately for data corrected by W2003, A2005, V2007, and CC2010 to obtain the C_{WEI}, C_{ARN}, C_{VIR}, and C_{COL} respectively. The C_{ref} was also determined for data, which were not corrected for the filter loading (C_{NC}, where subscript NC stands for "not corrected"). Because the MAAP measures the $\sigma_{abs,ref}$ only on the wavelength 637 nm, the closest AE31 and nephelometer data were first interpolated to the same wavelength. The σ_{ATN} and *ATN* measured by the AE31 and the σ_{sca} were interpolated to 637 nm by applying the Ångström exponent explained in Eq. 16. Also, the wavelength dependent constants used in W2003 and A2005 were interpolated to 637 nm. The *f* used in W2003 at 637 nm was 1.12 and the $a_{s,ARN}$ and $\tau_{a,fx}$ used in A2005 were 0.0681 and 0.2009 at 637 nm, respectively.

In the A2005, cumulative optical properties of the particles collected on the filter were needed, and thus the C_{ARN} was determined by iterating; the C_{ARN} was iterated for each filter spot until the median $\sigma_{abs,ref}$ and $\sigma_{abs,ARN}$ agreed within 1% limit. Because of the iteration, there is one C_{ARN} value for each filter spot. For other correction algorithms, the C_{ref} value was determined by two methods: 1) a linear fit to $\sigma_{ATN}(R(ATN))^{-1}$ vs. $\sigma_{abs,ref}$ to acquire the C_{ref} value for the whole data set; and by 2) simply using the Eq.19 to acquire the C_{ref} value for each measurement point separately. In the A2005, the C_{ARN} depends on the wavelength. In this study the C_{ARN} was determined only at the 637 nm. Since we followed a similar procedure as presented by Arnott et al. (2005), a fraction of the σ_{sca} was first subtracted from the σ_{ATN}, before determining the C_{ARN}, which is different to Eq. 19.

4 Results and discussion

4.1 Multiple scattering correction for the AE31

The different C_{ref} values were determined by a linear fit for loading corrected AE31 data vs. reference data from MAAP. Since the C_{ref} is described only by the slope of the fit, the intercept in the y-axis of the fit was forced to be zero. For the linear fit we used all the available data. The C_{ref} values were 3.00, 3.14, 2.99, and 2.77 for data corrected by W2003, V2007, CC2010, and for data that was not corrected, respectively.

https://doi.org/10.5194/amt-2020-325
Preprint. Discussion started: 8 September 2020


Atmospheric Measurement Techniques Discussions

Since the C_{ARN} was determined in an iterative manner for each filter spot, the C_{ARN} was calculated as the median of all of the filter spots and the resulted value was 3.13, which is shown in Table 2. Unlike the other algorithms, the A2005 assumed a wavelength dependent C_{ARN}. Here, we were only able to determine the C_{ref} at one wavelength by comparing the interpolated AE31 data to the MAAP measurements at 637 nm so we could not measure the C_{ARN} at different wavelengths. To acquire the C_{ARN} at all the seven wavelengths of the AE31, we used the power law function $C_{ARN}(\lambda) = C_{ARN,637nm}(\lambda/637\ nm)^{0.181} = 3.13 \cdot (\lambda/637\ nm)^{0.181}$, where the exponent 0.181 was obtained from a power function fitting to C_{ref} vs. λ in Table 1 of Arnott et al. (2005), similar to Virkkula et al. (2011). $C_{ARN,637nm} = 3.13$ is the value determined above at $\lambda = 637$ nm. The results of the wavelength dependent C_{ARN} values are presented in Table 2.

The smallest determined C_{ref} value was C_{NC}, which was expected. Since the σ_{ATN} decreases for a loaded filter and the filter loading correction was not applied, the C_{NC} has to be smaller than for the corrected data. The C_{NC} was considerably lower than for example the C_{WEI} and C_{COL}, which were about 8% higher than the C_{NC}. Since the values of the C_{WEI} and C_{COL} were almost the same, the result suggests that on average, the loading corrections R_{WEI} and R_{COL} had similar effects on the data. The highest values were determined for C_{VIR} and C_{ARN}, which were about 13% higher than C_{NC}. The C_{ARN} was determined differently (iterative process for each filter spot) than other C_{ref} values, which may partly explain the higher values. The C_{VIR}, however was determined similarly to C_{WEI} and C_{COL}. The reason for the higher C_{VIR} value is that on average, the value of the R_{VIR} was lower than the R_{WEI} or R_{COL} (i.e., the effect of filter loading correction in V2007 was stronger).

According to Collaud Coen et al. (2010), who studied the C_{ref} of different algorithms for ambient measurements in different kinds of environments, the higher C_{ref} values were typically measured in more polluted areas. Observations in our study support this claim. For example, they determined mean C_{WEI} of 2.81, 2.81, 3.05, and 4.09, at Hohenpeissenberg, Jungfraujoch, Mace Head, and Cabauw, respectively. Compared to their study the C_{ref} values at the SMEAR II were obviously lower than the mean C_{ref} values at the Cabauw measurement station, which is located near populated and industrial areas, and somewhat higher than in the clean mountain stations in Hohenpeissenberg and Jungfraujoch. The closest values were defined for the Mace Head station, which observes mostly marine air.

Backman et al. (2017) determined C_f (Backman et al. used the symbol C_f instead of C_{ref} to mark that the comparison was not conducted with a reference instrument) values for ambient data at several Arctic sites. They ran the comparison for Aethalometer data that were not corrected for the filter loading error. The median C_f values at 637 nm were 1.61, 3.12, 3.42, 4.01, and 4.22 measured at Summit, Barrow, Alert, Tiksi, and Pallas, respectively. Backman et al. (2017) did not find any clear explanation for the very low C_f at Summit. At the other sites, the C_f values were rather high compared to the C_{NC} observed at SMEAR II ($C_{NC} = 2.77$), which is unexpected if we would assume that the C_{ref} was lower at clean environments, such as Arctic, compared to sites closer to pollution sources.

https://doi.org/10.5194/amt-2020-325
Preprint. Discussion started: 8 September 2020


Atmospheric Measurement Techniques Discussions

In laboratory runs Arnott et al. (2005) determined C_{ref} = 2.076 (at 521 nm) for kerosene soot and Weingartner et al. (2003) observed C_{ref} = 2.14 (averaged over wavelengths) for not-coated soot particles. Compared to the C_{ref} determined in laboratory studies by Weingartner et al. (2003) and Arnott et al. (2005), the ambient measurements in our study yielded higher values. This was also observed by Arnott et al. (2005), who suggested C_{ref} = 3.688 (at 521 nm) for ambient measurements, which is closer to our observations. In addition to not-coated soot, Weingartner et al (2003) determined the C_{ref} for coated particles as well and the resulted C_{ref} was higher, about 3.6. This is also closer to our observations, which is probably explained by the fact that coated soot describes better the particles observed at SMEAR II, where the soot particles are likely aged and coated since there are no significant local emission sources.

The report 227 by WMO and GAW (World Meteorological Organization and Global Atmosphere Watch) recommends to determine the σ_{abs} from Aethalometer measurements by using C_{ref} value of 3.5 and not applying any filter loading correction or particle scattering reduction in the data. The C_{ref} was determined as an average over several datasets collected from different GAW stations. Comparing this value to the C_{NC}, using the recommended C_{ref} = 3.5 would systematically underestimate the σ_{abs} at SMEAR II by about 20%. It must be also noted, that due to the lack of $R(ATN)$ correction, the BC concentration or σ_{abs} may differ as much as 50% even if the real σ_{abs} would stay constant (Arnott et al., 2005). Therefore, in some cases, the data user may want to take the error caused by the filter loading into account and to use different correction algorithms. For example when studying shorter time periods (e.g., few days of data, which may fit few filter spot changes causing apparent variation in the measured concentration).

There are both studies where constant C_{ref} has been used and studies where wavelength dependent C_{ref} has been used. Others observed no significant dependency for the C_{ref} on the wavelength (Backman et al., 2017; Collaud Coen et al., 2010; Weingartner et al., 2003; WMO/GAW, 2016) and other studies observed the opposite and showed that the C_{ref} is wavelength dependent (Arnott et al., 2005; Kim et al., 2019; Schmid et al., 2006). These studies suggested that C_{ref} increases with wavelength (i.e. filter fibers scatter more light at longer wavelengths). It is worth pointing out that also Weingartner et al. (2003) presented slightly wavelength-dependent C_{ref} values, even though in the literature mainly their average value of 2.14 is cited. Interesting is also, that the wavelength dependency they obtained for internal mixtures of Diesel soot and ammonium sulfate and coated Palas soot yielded $C_{ref} = 3.9 \cdot (\lambda/660\ \text{nm})^{0.18}$ and $C_{ref} = 3.66 \cdot (\lambda/660\ \text{nm})^{0.23}$, respectively, as can be calculated from their Table 3. The exponents are very close to the value 0.18 obtained from the fittings to the Arnott et al. (2005) Table 1. Kim et al. (2019) found during the Cheju ABC Plume Monsoon EXperiment (CAPMEX) that C_{ref} depended on wavelength even more strongly, a fitting to their Table 2 yields $C_{ref} = 4.48(\lambda/532\text{nm})^{0.48}$. In these three studies, the absorption standard was a non-filterbased multiwavelength method.

The different C_{ref} values were not only determined as a linear fit averaging over the whole time series. In addition to the results from linear fits, the Table 2 presents the median, mean, and standard deviation of different C_{ref} values that were determined

https://doi.org/10.5194/amt-2020-325
Preprint. Discussion started: 8 September 2020


Atmospheric Measurement Techniques Discussions

separately for each data point according to Eq. 19. Determining the C_{ref} separately for each data point enabled studying the temporal variation of C_{ref}; for example the times series of the different C_{ref} values are presented in Fig. S1. The median and mean values differed somewhat from the slopes of the linear fits, which were about 10% lower than the median values. Comparing the median and mean values shows no large difference, meaning that the C_{ref} values were rather normally distributed. The variation of median C_{ref} values between the different correction algorithms was small compared to the relatively large standard deviation (see Table 2).

The C_{ref}, determined separately for each data point, was not stable over time (see time series presented in Fig. S1) and we observed seasonal variation for the C_{ref}, which is presented in Fig. 3 for the C_{NC}. The seasonal variation was not observed only for the C_{NC}, but also for the C_{WEI}, C_{ARN}, and C_{COL}, which is presented in Fig. S2. The seasonal variation of the C_{VIR} differed from the other algorithms so that the seasonal variation was not as clear. Figure 3 shows that the C_{NC} was clearly above the median during the summer and below the median in winter and early spring. The C_{NC} reached its maxima in July and its minima in February.

Since the C_{WEI}, C_{ARN}, and C_{COL} had a similar seasonal variation, it is unlikely that the seasonal variation observed for C_{NC} was caused by the lack of filter loading correction. It is actually rather surprising, that there was a seasonal variation for the C_{WEI}, C_{ARN}, and C_{COL} as well. A2005 and CC2010 took into account the ambient ω, which has a clear seasonal variation at SMEAR II (Luoma et al., 2019; Virkkula et al., 2011), but against the assumptions, this is not seen in the results. For example, the seasonal variations between the C_{WEI} and C_{COL} are surprisingly similar, even though we applied constant f values in W2003 However, the seasonal variation for C_{ARN} was a little less obvious than for C_{WEI}, C_{COL}, and C_{NC}, which might be because a fraction of the σ_{sca} was subtracted before the loading correction was applied and the C_{ARN} was determined. The lack of seasonal variation for C_{VIR} is probably caused by the very strong seasonal variation of the compensation parameter (k; see Fig. 10a) as will be discussed below. It seems that the V2007 is more dependent on the optical properties of the particles embedded in the filter than the other algorithms are and therefore the seasonal variation is reduced. The k is discussed more in Sect. 4.4.

The seasonal variations of the C_{ref} values might be explained by the fact that the C_{ref} is not necessarily a constant value, but it depends on the optical properties of the particles, which are embedded in the filter. As stated before, Weingartner et al. (2003) and Arnott et al. (2005) both observed different C_{ref} values for different types of aerosols so that the C_{ref} was lower for "pure" soot (no coating) and higher for coated soot or ambient aerosol particles. This would suggest that the C_{ref} increases with increasing ω. This supports our observations, since at SMEAR II the ω is the highest in summer and lowest in winter (Luoma et al., 2019; Virkkula et al., 2011). However, Collaud Coen et al. (2010) observed a decreasing trend for C_{ref} with increasing ω when they compared several stations.

https://doi.org/10.5194/amt-2020-325
Preprint. Discussion started: 8 September 2020


Atmospheric Measurement Techniques Discussions

The ω, however, is not the only optical property of aerosol particles that had a clear seasonal variation (Luoma et al., 2019; Virkkula et al., 2011). For example, the size dependent b and α_{sca} reach their maxima in summer and minima in winter, which indicates that in summer the particle size distribution had relatively more weight on smaller particles. Luoma et al. (2019) showed that the seasonal variation of b and α_{sca} is explained especially by the differences in accumulation mode (particles in the size range of 100 nm – 1 µm) particle concentration and size distribution: in summer, the volume concentration peaks around 250 nm and in winter around 350 nm. The size distribution affects the penetration depth of the particles as smaller particles penetrate deeper in the filter (Moteki et al., 2010). Scattering particles that penetrate deeper in the filter increase the multiple scattering in the filter, and that could be one explanation for higher C_{ref} values observed in summer.

The differences in the scattering properties of differently sized particles might also explain the observed seasonal variation of C_{ref}. The correction algorithms only take into account the amount of scattering, but not the direction of scattering. The smaller the particles are, the relatively more the particles scatter light in the backward direction increasing the optical path of the light ray through the filter (i.e. C_{ref} should increase). Therefore, this effect may cause the observed increase in the multiple scattering correction factor C_{ref} in summer. This could also explain why the C_{VIR} has no seasonal dependency; the compensation parameter seems to depend also on the b (see Sect. 4.4) and that would make the V2007 the only algorithm that takes the direction of the particulate scattering into account. Note that the V2007 does not take the b into account directly but it seems to have an effect on the calculated compensation parameter.

However, only weak correlation was found between the C_{NC} and ω (R = 0.17, p-value < 0.05), and C_{NC} and b (R = 0.23, p-value < 0.05), so there were only weak evidence on the dependency between the C_{ref} and optical properties of the aerosols, which could explain the seasonal variation of the C_{ref}. However, we observed moderate correlation (R = 0.30, p-value < 0.05) between the C_{ref} and RH measured in the MAAP, which is presented in Fig. 4 for the C_{NC} (the correlation was similar for C_{WEI}, C_{ARN}, C_{VIR}, and C_{COL} as well). Therefore, one possible reason for the observed seasonal variation of the different C_{ref} values could be caused by a technical issue, which is related to the difference in the relative humidity (RH) between the instruments. The RH presented in Fig. 4 was measured in the MAAP and it varied between 5 – 40%; for the AE31, the RH varied less and the RH was in the range of 5–20%. When the filter of the MAAP was exposed for RH equal or larger than 40%, the data was excluded from this study.

Figure 4 shows that the C_{NC} was higher when the sample air was more moist. The optical properties of the filter may change if the filter is exposed to high RH conditions. The aerosol particles may take up water even below super saturation and when the liquid particles collide on the filter the moisture is taken up by the filter. The RH may also affect the penetration depth of the particles in the filter, since the particles grow due to the water uptake (Moteki et al., 2010). When particles are penetrated deeper in the filter, the effect of the multiple scattering is higher increasing the measured σ_{ATN}. Because the RH in the MAAP was higher than in the AE31, the particles directed in the AE31 may have penetrated relatively deeper in the filter than the

https://doi.org/10.5194/amt-2020-325
Preprint. Discussion started: 8 September 2020


Atmospheric Measurement Techniques Discussions

particles directed in the MAAP filter. In winter, when the RH was low in both of the instruments the penetration depth would be more similar for each instrument. In summer, larger difference in the RH between the instruments could then increase the measured C_{ref}. This result shows that even though we have excluded the high *RH* data, the instruments seem to be sensitive to variations in RH even below the recommended 40%. However, the penetration depth depends also on the filter material, which is different for MAAP and AE31. Further analysis is omitted here.

4.2 Performance of the correction algorithms

Since the σ_{abs} derived from AE31 measurements used the C_{ref} values determined here, the σ_{abs} measurements of AE31 and MAAP were expected to agree well, which is shown in Fig. 5. The AE31 data in Fig. 5 was produced by applying the C_{ref} values determined from the linear fits (Table 2 column "fit"). The correlation coefficients and slopes of the linear fits presented in Fig. 5 were close to unity. However, all the AE31 correction schemes underestimateded the σ_{abs} a bit and the slopes varied from 0.93 to 0.97. The AE31 data corrected with the A2005 and CC2010 underestimated the σ_{abs} the most (slopes of the linear fits were 0.93). The reduction of particulate scattering in CC2010 after applying the multiple scattering correction (i.e., C_{ref}) explains the underestimation in CC2010 derived data. For the underestimation in A2005 derived data, the reason is probably the different way of determining the C_{ARN} compared to other C_{ref} values. The iterative manner of determining the C_{ARN} separately for each filter spot and then taking the median from these values was not as successful as the linear fit –method, which was used for the other algorithms.

Surprisingly, the not corrected AE31 (Fig. 5e) did not seem to have a significant difference in correlation coefficient compared to for example to the data corrected with W2003 or CC2010 (Figs. 5a and d, respectively). However, the relation between the $\sigma_{abs,NC}$ and σ_{ref} seemed to depend more on the *ATN* than for any filter loading corrected data, which is shown by the color coding (*ATN*) of the data points. If only data from highly loaded filter (*ATN* > 60) were taken into account, the slopes of the linear fits were 0.92, 1.00, 0.96, 0.90, and 0.88 for W2003, A2005, V2007, CC2010, and not corrected (NC), respectively. The smallest decrease in the slope determined for the loaded filter was observed for data that was corrected by V2007. Interestingly, the slopes for the loaded filter actually increased for data that was corrected by A2005, meaning that the R_{ARN} had a relatively big effect with increasing *ATN*. The biggest decrease in the slope determined for a highly loaded filter was observed for the not corrected data, as expected. This observation underlines the need for filter loading correction if one studies shorter time periods. For longer time periods (e.g., trend analysis or studies of seasonal variation) the effect of the *ATN* smooths out, but for shorter time periods (e.g., case studies) the changing *ATN* can have a notable effect on the results if no filter loading correction is applied.

The comparison between the MAAP and the PSAP is presented in Figs. 6a and b for both the correction schemes B1999 and V2010, respectively. The figure shows that V2010 overestimated the σ_{abs} when the *Tr* was low. For the whole data set the slope

https://doi.org/10.5194/amt-2020-325
Preprint. Discussion started: 8 September 2020


Atmospheric Measurement Techniques Discussions

of the linear regression was 1.24. If we calculate the linear regression for clean filter situations, when the $Tr > 0.7$ (at 660 nm), the slope of the linear fit is 1.01. For more loaded filter, with a limit of $Tr > 0.5$ (at 660 nm), the slope is 1.08.

The differences between these two correction algorithms are studied in more detail in Fig. 6c, which shows how the algorithms perform with different Tr and ω values. The figure shows that the V2010 produces notably higher σ_{abs} values when the filter is highly loaded ($Tr < 0.5$). The difference between the algorithms depends also on the ω so that at high ω and Tr, $\sigma_{abs,PSAP,VIR}/\sigma_{abs,PSAP,BON} < 1$ and when ω decreases the $\sigma_{abs,PSAP,VIR}/\sigma_{abs,PSAP,BON}$ ratio grows. The reason is that the V2010 algorithm is a function of ω.

4.3 Absorption Ångström exponent for different correction algorithms

The effect of the correction algorithms on α_{abs} were studied and the average α_{abs} for different correction algorithms of the AE31 and PSAP are presented in Fig. 7. For a comparison, the α_{abs} was also determined for the "raw" PSAP data that was not corrected by any algorithms (i.e., σ_{ATN}, see Eq. 1). To have comparable α_{abs} from the different instruments, Fig. 7 included only overlapping AE31 and PSAP data from 2011 – 2015. Since the PSAP operates at three wavelengths (467, 530, and 660 nm), we determined the AE31-related α_{abs} in Fig. 7 by using only the wavelengths 470, 520, 590, and 660 nm of the AE31. The rest of the AE31 wavelengths were omitted from this comparison to minimize the effect of different wavelength ranges have on α_{abs} (for example, see Luoma et al. (2019) Table 1). The α_{abs} was determined as -1×-slope of a linear fit to $\log(\sigma_{abs})$ vs. $\log(\lambda)$ over the selected wavelengths. Since Luoma et al. (2019) did not observe a big difference between the PM1 and PM10 α_{abs}, we included both measurements in this comparison.

According to Fig. 7, the median values of α_{abs} varied notably between the different instruments and correction algorithms: the lowest median value of α_{abs} was 0.85 and it was measured by AE31 and corrected by the CC2010; and the highest median value of α_{abs} was 1.48 and it was measured by PSAP and corrected by the V2010. The difference between the highest and lowest median values of α_{abs} was about 1.7-fold. The correction algorithms were applied to each wavelength separately and therefore the correction algorithms affected the wavelength dependency of the derived σ_{abs}. The scattering and loading corrections are different for each wavelength because for example the σ_{sca}, ω, ATN, and Tr, which are used in the algorithms, are wavelength dependent.

For the AE31, we studied the same five correction algorithms as in Sect. 4.1. The lowest median α_{abs} values were observed for the not corrected data ($\alpha_{abs,AE,NC}$) and for data that were corrected with the CC2010 and W2003 algorithms ($\alpha_{abs,\ AE,COL}$ and $\alpha_{abs,\ AE,WEI}$). The median α_{abs} values for the data corrected with A2005 and 2007 algorithms ($\alpha_{abs,\ AE,ARN}$ and $\alpha_{abs,\ AE,VIR}$) were higher, 1.20 and 1.19, respectively. Since we did not have reference measurements on several wavelengths, it is impossible to say which one of the correction algorithms yielded the most truthful value for the α_{abs}. This could be done with several MAAPs

https://doi.org/10.5194/amt-2020-325
Preprint. Discussion started: 8 September 2020


Atmospheric Measurement Techniques Discussions

operating at different wavelengths or by measuring the particles suspended in the air by photoacoustic method (Kim et al., 2019).

The A2005 was the only algorithm that assumed a wavelength dependent C_{ref}. Since the C_{ARN} increased with wavelength (i.e., bigger correction due to multiple scattering at higher wavelengths), taking the wavelength dependency of the C_{ref} into account increases the $\alpha_{abs,\,AE,ARN}$ compared to other algorithms. The correction factor of the V2007 algorithm depended on the difference between the *ATN* of loaded and clean filter spots. Most of the time *ATN* increased faster at short wavelengths than at long wavelengths, so the difference between the *ATN* of the loaded and clean filter spots was higher than for longer wavelengths. Therefore, the filter loading correction was bigger for shorter wavelengths and after the correction the difference between the σ_{abs} at different wavelengths increased, increasing the α_{abs} as well.

For the PSAP data, the α_{abs} were generally a bit higher compared to the AE31 derived α_{abs}. The lowest PSAP derived median value for $\alpha_{abs\ PSAP,NC}$ was 1.01, which resulted from data that was not corrected by any algorithm. B1999 resulted for median $\alpha_{abs,PSAP,BON}$ value of 1.04, and the V2010 produced the overall the highest $\alpha_{abs,PSAP,VIR}$, which was 1.48. Similar order of the average α_{abs} from different algorithms was observed by Backman et al. (2014) at an urban station in Elandsfontein, South Africa. For a dataset measured off the east coast of the United States on a research ship, Backman et al. (2014) reported also the highest α_{abs} for the V2010. These results are consistent with each other. The explanation is that in V2010 all constants are wavelength dependent, contrary to the B1999.

We also studied if the α_{abs} values were affected as the filter got more loaded with particles. Figure 8 presents the α_{abs} derived from AE31 data corrected with different algorithms as a function of *ATN* and Fig. 9 presents the α_{abs} derived from PSAP data as a function of *Tr*. The α_{abs} derived from corrected PSAP data (Fig. 9a and b) did not seem to depend on loading at $Tr > 0.4$ but for higher filter loadings the α_{abs} growed with decreasing *Tr* with both B1999 and V2010 corrections. As a comparison, for the not corrected PSAP data (i.e., σ_{ATN}), the α_{abs} decreased with increasing *Tr* (Fig. 9c). The α_{abs} derived from the AE31 data was also studied; the $\alpha_{abs,AE,WEI}$, $\alpha_{abs,AE,ARN}$, $\alpha_{abs,AE,COL}$, and $\alpha_{abs,AE,NC}$ clearly decreased with increasing *ATN*. If the *ATN* increased from 5 to 70, the decreases in $\alpha_{abs,\,AE,WEI}$, $\alpha_{abs,AE,ARN}$, $\alpha_{abs,\,AE,COL}$, and $\alpha_{abs,\,AE,NC}$ were rather linear and the decreases were around -22, -23, -33, and -27%, respectively.

The $\alpha_{abs,AE,VIR}$, derived from data corrected with V2007, did not seem to depend on the *ATN*, if not taking into account very high filter loadings ($ATN > 70$). In V2007, the *k* was determined for each wavelength separately. In the next chapter, we show that the *k* is typically largest for the shorter wavelengths, which means that the nonlinearity caused by the increased filter loading is relatively stronger at the shorter wavelengths. When this is not taken into account, the α_{abs} decreases with the increasing *ATN*, which is seen with the other algorithms.

https://doi.org/10.5194/amt-2020-325
Preprint. Discussion started: 8 September 2020


Atmospheric Measurement Techniques Discussions

4.4 Variations of the compensation parameter

The variation of *k* at SMEAR II has already been studied by Virkkula et al. (2007) who used AE31 data from December 2004 to September 2006. During this period, the AE31 was operating without any cut-off and there were no scattering measurements available, and this period was not included in our study. Here, we repeated the analysis for a longer time series and included the σ_{sca} measurements, so we could also determine the *b* and ω.

The average values of the *k* are presented in Table 4. The mean values of the *k* varied from $4.6 \cdot 10^{-3}$ at 370 nm to $2.0 \cdot 10^{-3}$ at 950 nm. The wavelength dependency of *k* is described by a_k, which is the slope of a linear fit of the *k* over different wavelengths ($k_\lambda = a_k\lambda + k_0$, see example in Fig. 10b). Negative a_k means that on average the filter loading correction was greater at shorter wavelengths. The light attenuation is stronger at shorter wavelengths due to higher absorption and scattering by the particles and therefore the shorter wavelengths are prone to bigger error caused by the filter loading. At longer wavelengths, the standard deviation of the *k* was higher, meaning that the *k* was more sensitive to the particle properties at longer wavelengths. The same observation was noted by Virkkula et al. (2015) as well.

At SMEAR II, we observed that the *k* and the a_k had a very strong seasonal variation so that the *k* and a_k were the lowest in summer, which was also noted by Virkkula et al. (2007). The seasonal variation was observed at all wavelengths, but the variation was more pronounced at longer wavelengths. The seasonally averaged *k* and a_k are presented in Table 4 and an example of the seasonal variation of *k* at 880 nm is presented in Fig. 10a. Similar seasonal pattern for the *k* were also observed by Virkkula et al. (2007), Wang et al. (2011), and Song et al. (2013). In summer, the mean *k* values at the longer wavelengths (660–950 nm) were actually negative, meaning that without the correction, the AE31 would actually overestimate the σ_{abs} at longer wavelengths.

Previous studies (e.g., Virkkula et al., 2007; Wang et al., 2011; and Song et al., 2013) suggested that the seasonal variation in *k* could be due to variations in ω, so that lower ω induced higher *k*. This correlation is observed at SMEAR II as shown in Figs. 10a and d; the ω peaks in summer as the *k* has its minima and the correlation coefficient between the ω and *k* is -0.47. The variation of ω also explains the observed negative *k* values. Virkkula et al. (2007) stated that the negative values are associated with the response of the Aethalometer to scattering aerosols as the negative *k* are observed when the ω is high. The effect of ω was taken into account for example in the AE31 correction algorithms suggested by Weingartner et al. (2003), Arnott et al. (2007), and Collaud Coen et al. (2010). Virkkula et al. (2015) presented a theoretical explanation to the ω dependency of *k*, which our analysis supports.

Also, the effect caused by the sizes of the particles has been suggested. The particle sizes affect the scattering properties of the particles and also an effect on the penetration depth in the filter, which could affect the *k*. The size distribution of the particle

https://doi.org/10.5194/amt-2020-325
Preprint. Discussion started: 8 September 2020


Atmospheric Measurement Techniques Discussions

population is described by the *b* so that higher *b* indicates smaller particles. Müller et al. (2014), for example, showed that the effect of asymmetry parameter, which is a function of *b* (Andrews et al., 2006), had an effect on the PSAP data.

The dependency of *k* on both *b* and ω was investigated more closely by Virkkula et al. (2015) at SORPES, an urban station located in Nanjing, China. The study showed positive correlation between *k* and *b*, and negative correlation between *k* and ω. At SMEAR II, we also observed negative correlation between *k* and ω (Fig. 10c). However, contrary to the results by Virkkula et al. (2015), we observed negative correlation between *k* and *b* (Fig. 10d). Virkkula et al. (2015) discussed about the difficulties to show whether the *b* or the ω was the dominant property in determining the *k*. At SMEAR II, the ω varies in a wider range compared to the observations at SORPES, which could explain some of the observed differences. The mean and standard deviation of ω at SMEAR II were 0.87 ± 0.07 (at 550 nm; Luoma et al., 2019) and at SORPES 0.93 ± 0.03 (at 520 nm; Shen et al., 2018). However, a clear reason for the negative correlation between the *k* and *b* at SMEAR II was not found.

5 Summary and conclusions

In this study, we presented a comparison of three different absorption photometers (AE31, PSAP, and MAAP), which measured ambient air at SMEAR II, a rural station located in middle of a boreal forest in southern Finland. We also compared different correction algorithms that are used in determining the absorption coefficient (σ_{abs}) from the raw absorption photometer data. We studied how the algorithms affected the derived parameters and determined multiple scattering correction factor (C_{ref}) applicable at SMEAR II.

To get more reliable AE31 measurements, the AE31 data were compared against the MAAP data to acquire the C_{ref} that is used in the processing of the AE31 data. The resulted C_{ref} values were 3.00, 3.13, 3.14, and 2.99 for the algorithms suggested by Weingartner et al. (2003), Arnott et al. (2005), Virkkula et al. (2007), and Collaud Coen et al. (2010), respectively. Previous studies observed that the C_{ref} varied between different types of environments and stations and here it was determined for the SMEAR II station, which represents the atmospheric conditions in a boreal forest. The C_{ref} determined at the SMEAR II can be applied to other boreal forest sites as well. Even though the AE31 is the an old model and no longer in production, the results can be used in post-processing older data sets or at sites that still operate the older AE31. Newer model of the Aethalometer, AE33, applies the so-called dual-spot correction so the instrument operators do not need to apply the correction algorithms themselves. However, the value of C_{ref} is an open question for the AE33 also but since its filter material is different from the one used in the AE31, the results of the present study are not applicable to it.

We observed also a clear seasonal cycle associated with C_{ref}, which was probably due to the variations in the optical properties of the aerosol particles, such as the *b* and ω. We also observed some correlation between the C_{ref} and *RH* even though the *RH*

https://doi.org/10.5194/amt-2020-325
Preprint. Discussion started: 8 September 2020


Atmospheric Measurement Techniques Discussions

in the instruments were kept below 40%. These results show that the filter measurement methods seem to be rather sensitive to the *RH* even if the *RH* is below the recommended value of 40%.

The results obtained for data corrected with the algorithm by Virkkula et al. (2007) were in many ways different from those obtained by Collaud Coen et al. (2010) who applied the Virkkula et al. (2007) correction to data from several stations in Europe. They found that the compensation parameter (*k*) used in the algorithm was highly nonstable and that it led to large outliers. They correctly stated that the difficulty of applying this correction is due to the natural high variability of σ_{ATN} as a function of time, which is for most of the time greater than the σ_{ATN} decrease induced by filter changes. We therefore calculated 14-day running average compensation parameters (±7 days around each filter spot) in order to minimize these problems. The approach was obviously successful. It can be recommended that users of this method calculate running averages of *k*. However, no exact time span can be given, it depends on the concentration level of the measurement site – at a clean site like SMEAR II 14 days was sufficient and in the polluted Nanjing 24 hours.

The results showed a great variation between the α_{abs} derived from differently corrected σ_{abs} data and at SMEAR II the median α_{abs} for different algorithms varied in the range of 0.93 – 1.54. We also observed that most of the correction methods did not prevent the change in the wavelength dependency as the filter got more loaded and therefore the α_{abs} decreased notably with increasing attenuation (*ATN*). The correction algorithm by Virkkula et al., (2007) was the only AE31 correction algorithm, which produced a stable α_{abs} for the increasing filter loading. For example, the α_{abs} derived from Aethalometer measurements is often used to describe the chemical properties of the particles and to describe the source of black carbon. Not taking the used correction algorithm and the effect of increasing filter loading into account, could lead to wrong interpretation of the results. According to our results, applying the Virkkula et al. (2007) correction algorithm could help solving if the changes in α_{abs} were due to real variation or due to increased filter loading.

In general, the results showed that applying a filter loading correction to AE31 data clearly reduces the effect of increasing filter attenuation (*ATN*) and therefore applying a correction to the data is especially important, if the data is studied for shorter periods. When applying a correction algorithm to AE31 data, it is important to report which algorithm, C_{ref} values and other coefficients were used to acquire the final data product, since the algorithms can have a notable effect on the results, especially the absorption Ångström exponent α_{abs}. Our results showed that it is a good practice to perform the analysis of AE31 data by using few different correction algorithms, to see if the results vary notably for different algorithms.

Author contributions

KL performed the data analysis and wrote the paper together with AV. PA and AV have set up the aerosol optical measurements at SMEAR II. All authors reviewed and commented on the paper.

https://doi.org/10.5194/amt-2020-325
Preprint. Discussion started: 8 September 2020

Acknowledgements

We thank SMEAR II staff for taking care that all the measurements were running.

Financial support

This research has been supported by the European Union's Horizon 2020 research and innovation program via projects ACTRIS-2 (grant no. 654109) and iCUPE (grant no. 689443). Additional financial support was received through the Academy of Finland (Center of Excellence in Atmospheric Sciences) under the projects PROFI-3 (decision no. 311932), NANOBIOMASS (decision no. 307537). This research was also supported by Academy of Finland via project NABCEA (grant no. 29664) and by Business Finland via project BC Footprint (grant no. 49402-201040). Financial support of University of Helsinki to ACTRIS-FI is gratefully acknowledged.

References

Anderson, T., Covert, D., Marshall, S., Laucks, M., Charlson, R., Waggoner, A., Ogren, J., Caldow, R., Holm, R., Quant, F., Sem, G., Wiedensohler, A., Ahlquist, N., and Bates, T.: Performance characteristics of a high-sensitivity, three-wavelength, total scatter/backscatter nephelometer, J. Atmos. Ocean Tech., 13, 967-986, 1996.

Anderson, T. L., and Ogren, J. A.: Determining aerosol radiative properties using the TSI 3563 integrating nephelometer, Aerosol Sci. Technol., 29, 57-69, 10.1080/02786829808965551, 1998.

Andrews, E., Sheridan, P., Fiebig, M., McComiskey, A., Ogren, J., Arnott, P., Covert, D., Elleman, R., Gasparini, R., and Collins, D.: Comparison of methods for deriving aerosol asymmetry parameter, J. Geophys. Res. Atmos., 111, 10.1029/2004JD005734, 2006.

Arnott, W. P., Hamasha, K., Moosmüller, H., Sheridan, P. J., and Ogren, J. A.: Towards aerosol light-absorption measurements with a 7-wavelength Aethalometer: Evaluation with a photoacoustic instrument and 3-wavelength nephelometer, Aerosol Sci. Technol., 39, 17-29, 10.1080/027868290901972, 2005.

Backman, J., Virkkula, A., Vakkari, V., Beukes, J., Van Zyl, P., Josipovic, M., Piketh, S., Tiitta, P., Chiloane, K., Petäjä, T., Kulmala, M., and Laakso, L.: Differences in aerosol absorption Ångström exponents between correction algorithms for a particle soot absorption photometer measured on the South African Highveld, Atmos, Atmos. Meas. Tech., 7, 4285-4298, 10.5194/amt-7-4285-2014, 2014.

Backman, J., Schmeisser, L., Virkkula, A., Ogren, J. A., Asmi, E., Starkweather, S., Sharma, S., Eleftheriadis, K., Uttal, T., Jefferson, A., Bergin, M., Makshtas, A., Tunved, P., and Fiebig, M.: On Aethalometer measurement uncertainties and an instrument correction factor for the Arctic, Atmos. Meas. Tech., 10.5194/amt-10-5039-2017, 2017.

Bond, T. C., Anderson, T. L., and Campbell, D.: Calibration and intercomparison of filter-based measurements of visible light absorption by aerosols, Aerosol Sci. Technol., 30, 582-600, 10.1080/027868299304435, 1999.

Bond, T. C., Covert, D. S., and Müller, T.: Truncation and angular-scattering corrections for absorbing aerosol in the TSI 3563 nephelometer, Aerosol Sci. Technol., 43, 866-871, 10.1080/02786820902998373, 2009.

Collaud Coen, M., Weingartner, E., Apituley, A., Ceburnis, D., Fierz-Schmidhauser, R., Flentje, H., Henzing, J., Jennings, S. G., Moerman, M., Petzold, A., Schmid, O., and Baltensperger, U.: Minimizing light absorption measurement artifacts of the Aethalometer: evaluation of five correction algorithms, Atmos. Meas. Tech., 3, 457-474, 10.5194/amt-3-457-2010, 2010.

Hari, P., and Kulmala, M.: Station for measuring ecosystem–atmosphere relations, Boreal Environ. Res., 10, 315-322, 2005.

Hari, P., Nikinmaa, E., Pohja, T., Siivola, E., Bäck, J., Vesala, T., and Kulmala, M.: Station for measuring ecosystem-atmosphere relations: SMEAR, in: Physical and Physiological Forest Ecology, Springer, 471-487, 2013.

Haywood, J., and Shine, K.: The effect of anthropogenic sulfate and soot aerosol on the clear sky planetary radiation budget, Geophys. Res. Lett., 22, 603-606, 10.1029/95GL00075, 1995.

Hyvärinen, A., Vakkari, V., Laakso, L., Hooda, R., Sharma, V., Panwar, T., Beukes, J., van Zyl, P., Josipovic, M., Garland, R. M., Andreae, M. O., Pöschl, U., and Petzold, A.: Correction for a measurement artifact of the Multi-Angle Absorption 483 Photometer (MAAP) at high black carbon mass concentration levels, Atmos. Meas. Tech., 6, 81-90, 10.5194/amt-6-81-2013, 2013.

Kebabian, P. L., Robinson, W. A., and Freedman, A.: Optical extinction monitor using cw cavity enhanced detection, Rev. Sci. Instrum., 78, 063102, 10.1063/1.2744223, 2007.

Kim, J.-H., Kim, S.-W., Ogren, J. A., Sheridan, P. J., Yoon, S.-C., Sharma, S., and Lin, N.-H.: Multiple scattering correction factor estimation for aethalometer aerosol absorption coefficient measurement, Aerosol Sci. Technol., 53, 160-171, 10.1080/02786826.2018.1555368, 2019.

Li, H., McMeeking, G. R., and May, A. A.: Development of a new correction algorithm applicable to any filter-based absorption photometer, Atmos. Meas. Tech., 13, 2865-2886, 10.5194/amt-13-2865-2020, 2020.

Lohmann, U., and Feichter, J.: Global indirect aerosol effects: A review, Atmos. Chem. Phys., 5, 715-737, 10.5194/acp-5-715-2005, 2005.

Luoma, K., Virkkula, A., Aalto, P., Petäjä, T., and Kulmala, M.: Over a 10-year record of aerosol optical properties at SMEAR II, Atmos. Chem. Phys., 19, 11363-11382, 10.5194/acp-19-11363-2019, 2019.

Moteki, N., Kondo, Y., Nakayama, T., Kita, K., Sahu, L. K., Ishigai, T., Kinase, T., and Matsumi, Y.: Radiative transfer modeling of filter-based measurements of light absorption by particles: Importance of particle size dependent penetration depth, J. Aerosol Sci, 41, 401-412, 10.1016/j.jaerosci.2010.02.002, 2010.

Müller, T., Henzing, J., De Leeuw, G., Wiedensohler, A., Alastuey, A., Angelov, H., Bizjak, M., Coen, M., Engstrom, J., Gruening, C., Hillamo, R., Hoffer, A., Imre, K., Ivanow, P., Jennings, G., Sun, J., Kalivitis, N., Karlsson, H., Komppula, M., Laj, P., Li, S.-M., Lunder, C., Marinoni, A., Martins dos Santos, S., Moerman, M., Nowak, A., Ogren, J., Petzold, A., Pichon, J., Rodriquez, S., Sharma, S., Sheridan, P., Teinilä, K., Tuch, T., Viana, M., Virkkula, A., Weingartner, E., Wilhelm, R., and Wang, Y.: Characterization and intercomparison of aerosol absorption photometers: result of two intercomparison workshops, Atmos. Meas. Tech., 4, 245-268, 10.5194/amt-4-245-201, 2011a.

Müller, T., Laborde, M., Kassell, G., and Wiedensohler, A.: Design and performance of a three-wavelength LED-based total scatter and backscatter integrating nephelometer, Atmos. Meas. Tech., 4, 1291-1303, 10.5194/amt-4-1291-2011, 2011b.

Müller, T., Virkkula, A., and Ogren, J. A.: Constrained two-stream algorithm for calculating aerosol light absorption coefficient from the Particle Soot Absorption Photometer, Atmos. Meas. Tech., 7, 4049-4070, 10.5194/amt-7-4049-2014, 2014.

Ogren, J. A.: Comment on "Calibration and intercomparison of filter-based measurements of visible light absorption by aerosols", Aerosol Sci. Technol., 44, 589-591, 10.1080/02786826.2010.482111, 2010.

Petzold, A., and Schönlinner, M.: Multi-angle absorption photometry—a new method for the measurement of aerosol light absorption and atmospheric black carbon, J. Aerosol Sci, 35, 421-441, 10.1016/j.jaerosci.2003.09.005, 2004.

Sandradewi, J., Prévôt, A. S., Szidat, S., Perron, N., Alfarra, M. R., Lanz, V. A., Weingartner, E., and Baltensperger, U.: Using aerosol light absorption measurements for the quantitative determination of wood burning and traffic emission contributions to particulate matter, Environ. Sci. Technol., 42, 3316-3323, 10.1021/es702253m, 2008.

Schmid, O., Artaxo, P., Arnott, W. P., Chand, D., Gatti, L. V., Frank, G. P., Hoffer, A., Schnaiter, M., and Andreae, M. O.: Spectral light absorption by ambient aerosols influenced by biomass burning in the Amazon Basin. I: Comparison and field calibration of absorption measurement techniques, Atmos. Chem. Phys., 6, 3443-3462, 10.5194/acp-6-3443-2006, 2006.

https://doi.org/10.5194/amt-2020-325
Preprint. Discussion started: 8 September 2020

Shen, Y., Virkkula, A., Ding, A., Wang, J., Chi, X., Nie, W., Qi, X., Huang, X., Liu, Q., Zheng, L., Zheng, X., Petäjä, T., Aalto, P., Fu, C., and Kulmala, M.: Aerosol optical properties at SORPES in Nanjing, east China, Atmos. Chem. Phys., 18, 5265-5292, 10.5194/acp-18-5265-2018, 2018.

Song, S., Wu, Y., Xu, J., Ohara, T., Hasegawa, S., Li, J., Yang, L., and Hao, J.: Black carbon at a roadside site in Beijing: Temporal variations and relationships with carbon monoxide and particle number size distribution, Atmos. Environ., 77, 213-221, 10.1016/j.atmosenv.2013.04.055, 2013.

Stocker, T. F., Qin, D., Plattner, G.-K., Tignor, M., Allen, S. K., Boschung, J., Nauels, A., Xia, Y., Bex, V., and Midgley, P. M.: Climate change 2013: The physical science basis, 2013.

Wang, Y., Hopke, P. K., Rattigan, O. V., Xia, X., Chalupa, D. C., and Utell, M. J.: Characterization of residential wood combustion particles using the two-wavelength aethalometer, Environ. Sci. Technol., 45, 7387-7393, 10.1021/es2013984, 2011.

Weingartner, E., Saathoff, H., Schnaiter, M., Streit, N., Bitnar, B., and Baltensperger, U.: Absorption of light by soot particles: determination of the absorption coefficient by means of Aethalometers, J. Aerosol Sci, 34, 1445-1463, 10.1016/S0021-8502(03)00359-8, 2003.

Virkkula, A., Ahlquist, N. C., Covert, D. S., Arnott, W. P., Sheridan, P. J., Quinn, P. K., and Coffman, D. J.: Modification, calibration and a field test of an instrument for measuring light absorption by particles, Aerosol Sci. Technol., 39, 68-83, 10.1080/027868290901963, 2005.

Virkkula, A., Mäkelä, T., Hillamo, R., Yli-Tuomi, T., Hirsikko, A., Hämeri, K., and Koponen, I. K.: A simple procedure for correcting loading effects of Aethalometer data, J. Air Waste Ma., 57, 1214-1222, 10.3155/1047-3289.57.10.1214, 2007.

Virkkula, A.: Correction of the calibration of the 3-wavelength particle soot absorption photometer (3λ PSAP), Aerosol Sci. Technol., 44, 706-712, 10.1080/02786826.2010.482110, 2010.

Virkkula, A., Backman, J., Aalto, P., Hulkkonen, M., Riuttanen, L., Nieminen, T., Dal Maso, M., Sogacheva, L., De Leeuw, G., and Kulmala, M.: Seasonal cycle, size dependencies, and source analyses of aerosol optical properties at the SMEAR II measurement station in Hyytiala, Finland, Atmos. Chem. Phys., 11, 4445, 10.5194/acp-11-4445-2011, 2011.

Virkkula, A., Chi, X., Ding, A., Shen, Y., Nie, W., Qi, X., Zheng, L., Huang, X., Xie, Y., Wang, J., Petäjä, T., and Kulmala, M.: On the interpretation of the loading correction of the Aethalometer, Atmos. Meas. Tech., 8, 4415-4427, 10.5194/amt-8-4415-2015, 2015.

WMO/GAW: Aerosol measurement procedures, guidelines and recommendations, 2nd edition, GAW Report No. 227, World Meteorological Organization, Geneva, Switzerland, 2016.

Zotter, P., Herich, H., Gysel, M., El-Haddad, I., Zhang, Y., Močnik, G., Hüglin, C., Baltensperger, U., Szidat, S., and Prévôt, A. S.: Evaluation of the absorption Ångström exponents for traffic and wood burning in the Aethalometer-based source apportionment using radiocarbon measurements of ambient aerosol, Atmos. Chem. Phys., 17, 4229-4249, 10.5194/acp-17-4229-2017, 2017.

https://doi.org/10.5194/amt-2020-325
Preprint. Discussion started: 8 September 2020

Atmospheric Measurement Techniques Discussions

Table 1. All the wavelength dependent coefficients used in the AE31 correction algorithms proposed by Weingartner et al. (2003) and Arnott et al. (2005). Also, the extrapolated values of the multiple scattering correction factor used in the Arnott et al. (2005) correction algorithm (C_{ARN}) at different wavelengths are presented in the table.

Coefficients for AE31 correction algorithm by Weingartner et al. (2003)							
λ (nm)	370	470	520	590	660	880	950
a	0.88	0.87	0.86	0.86	0.85	0.83	0.82
ω	0.91	0.89	0.89	0.88	0.85	0.83	0.82
f	1.08	1.10	1.10	1.11	1.12	1.14	1.15
Coefficients for AE31 correction algorithm by Arnott et al. (2005)							
λ (nm)	370	470	520	590	660	880	950
$100 \cdot a_{s.ARN}$	3.35	4.57	5.23	6.16	7.13	10.38	11.48
$\tau_{a,fx}$	0.3026	0.2527	0.2338	0.2129	0.1956	0.1575	0.1486
C_{ARN}	2.70	2.82	2.87	2.94	3.00	3.16	3.20

Table 1. Average values for the multiple scattering correction factor (C_{ref}) for the different correction algorithms. These values are reported at the Aethalometer wavelength 637 nm. The slope of the fit and the standard error of the fit (SE) were determined by a linear regression applied for the whole data set. The median, mean, and stardard deviation (SD) were determined from the C_{ref} values that were calculated for each data point separately.

	fit	**SE**	**median**	**mean**	**SD**
C_{WEI}	3.00	0.003	3.34	3.29	0.57
C_{ARN}			3.13	3.13	0.45
C_{VIR}	3.14	0.002	3.30	3.28	0.56
C_{COL}	2.99	0.003	3.28	3.32	0.57
C_{NC}	2.77	0.003	3.09	3.06	0.55

https://doi.org/10.5194/amt-2020-325
Preprint. Discussion started: 8 September 2020

Atmospheric Measurement Techniques Discussions

Table 4. The mean compensation parameters (*k*) and the wavelength dependency of the *k* (a_k) for the AE31 correction algorithm suggested by Virkkula et al. (2007). The average values are calculated over all the seasons, but also separately for each season. The seasons were classified as: spring (March – May), summer (June – August), autumn (September – November), and winter (December – February).

Season	370 nm ($\cdot 10^{-3}$)	470 nm ($\cdot 10^{-3}$)	520 nm ($\cdot 10^{-3}$)	590 nm ($\cdot 10^{-3}$)	660 nm ($\cdot 10^{-3}$)	880 nm ($\cdot 10^{-3}$)	950 nm ($\cdot 10^{-3}$)	a_k ($\cdot 10^{-6}$ nm^{-1})
all	4.6 ± 7.0	3.6 ± 7.2	3.5 ± 8.0	3.4 ± 8.9	2.7 ± 9.5	2.1 ± 10.6	2.0 ± 10.8	-4.2
spring	4.4 ± 7.0	3.5 ± 6.5	3.4 ± 7.6	3.4 ± 8.8	2.8 ± 9.2	2.2 ± 10.5	2.2 ± 10.2	-3.5
summer	3.0 ± 6.7	1.5 ± 6.3	1.1 ± 6.9	0.5 ± 9.0	-0.4 ± 9.6	-1.7 ± 10.3	-2.5 ± 11.3	-8.8
autumn	4.6 ± 7.7	3.6 ± 9.1	3.6 ± 9.7	3.5 ±10.3	2.8 ±10.2	2.5 ± 10.9	2.2 ± 12.1	-3.6
winter	5.5 ± 6.3	4.8 ± 6.4	4.8 ± 7.0	4.8 ± 6.9	4.3 ± 8.4	4.4 ± 9.9	4.3 ± 9.1	-1.7

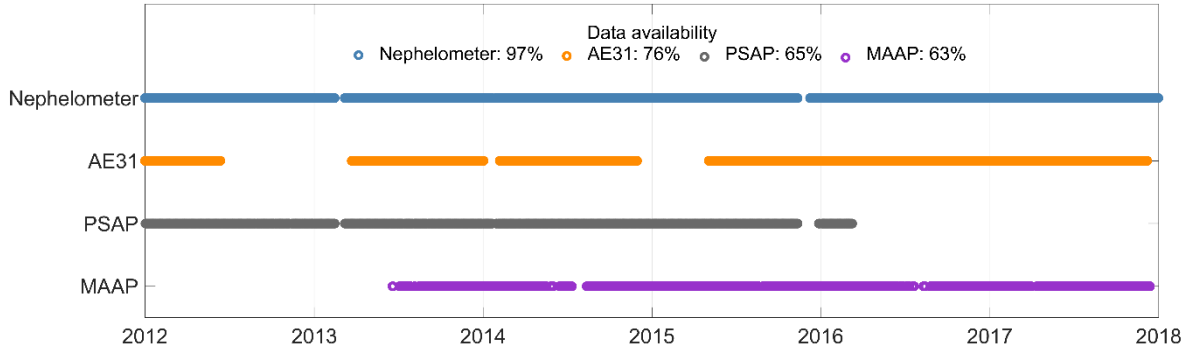

Figure 1: The availability of the optical aerosol data at SMEAR II station from the integrating nephelometer, AE31, PSAP, and MAAP. The dots represent days that had at least 50% of data available. The data availability for each instrument for the whole period of 2012 - 2017 is given in the legend.

https://doi.org/10.5194/amt-2020-325
Preprint. Discussion started: 8 September 2020

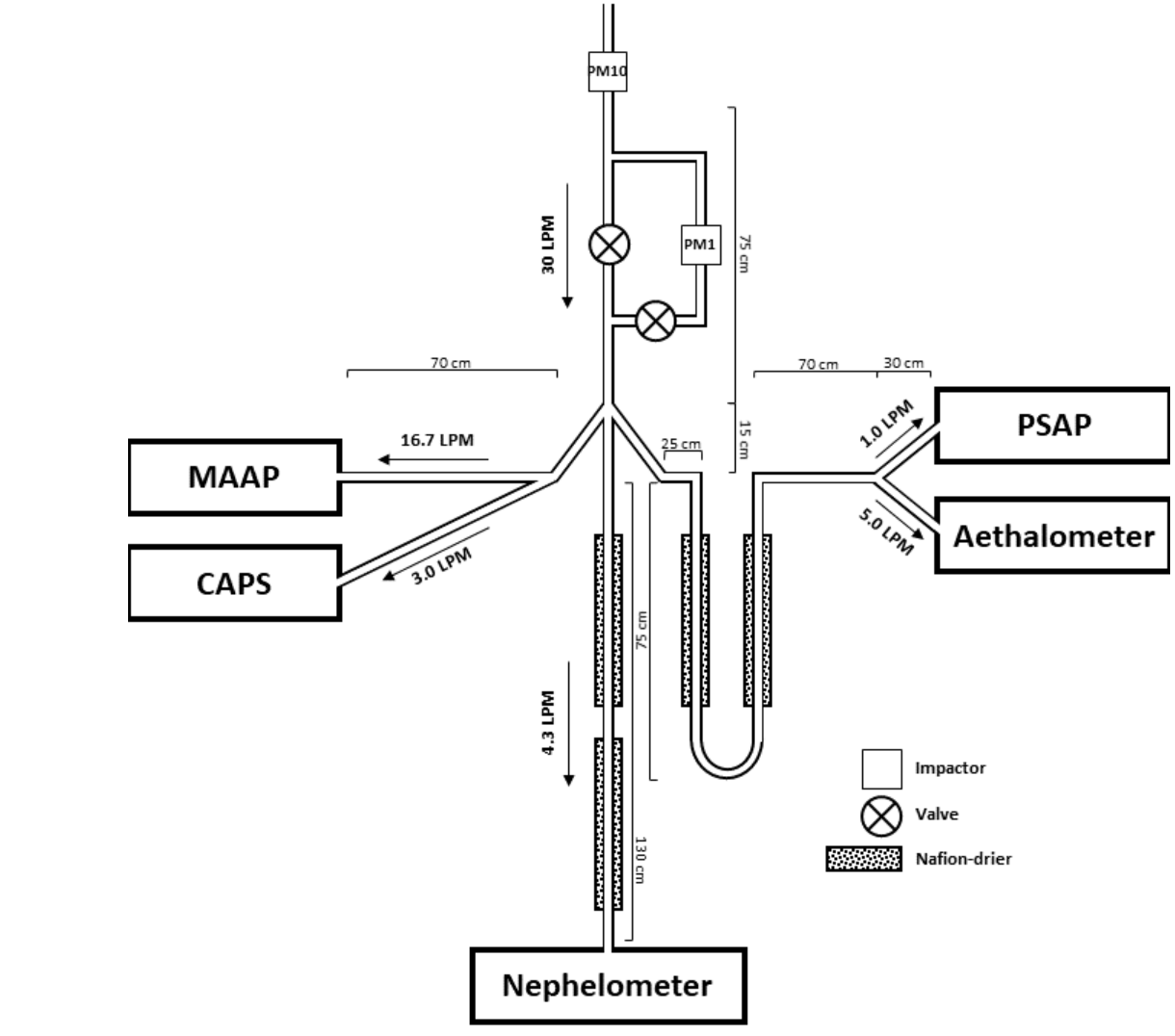

Figure 2: Measurement scheme for the instruments that measured the aerosol optical properties at the SMEAR II station. This setup was running during 2014–2015, when all the instruments were operating in parallel.

https://doi.org/10.5194/amt-2020-325
Preprint. Discussion started: 8 September 2020

Atmospheric Measurement Techniques Discussions

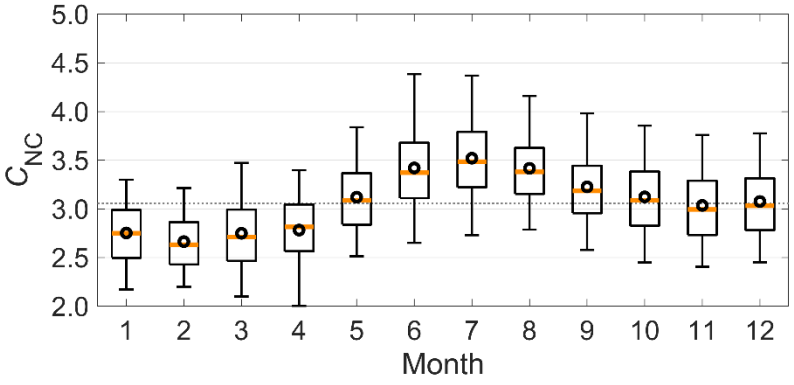

Figure 3. The seasonal variation of the multiple scattering correction factor for not corrected data (C_{NC}). The orange line in the middle of the box is the median, the black circle is the mean, the edges of the boxes represent the 25th and 75th percentiles, and the whiskers represent the 10th and 90th percentiles of the data. The median C_{NC} is presented with a dashed line.

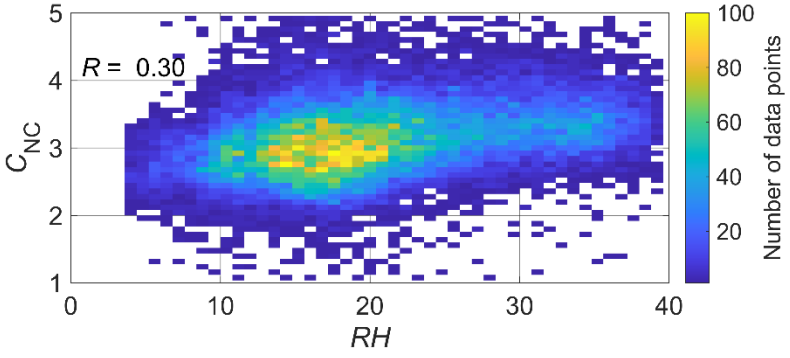

Figure 4. The dependency of the multiple scattering correction factor for not corrected data (C_{NC}) on the instrumental relative humidity (*RH*) in the MAAP. The colored grid points represent the number of data points in each grid point. There is 50 grid points in x- and y-directions so in total there are 2500 grid points.

https://doi.org/10.5194/amt-2020-325
Preprint. Discussion started: 8 September 2020

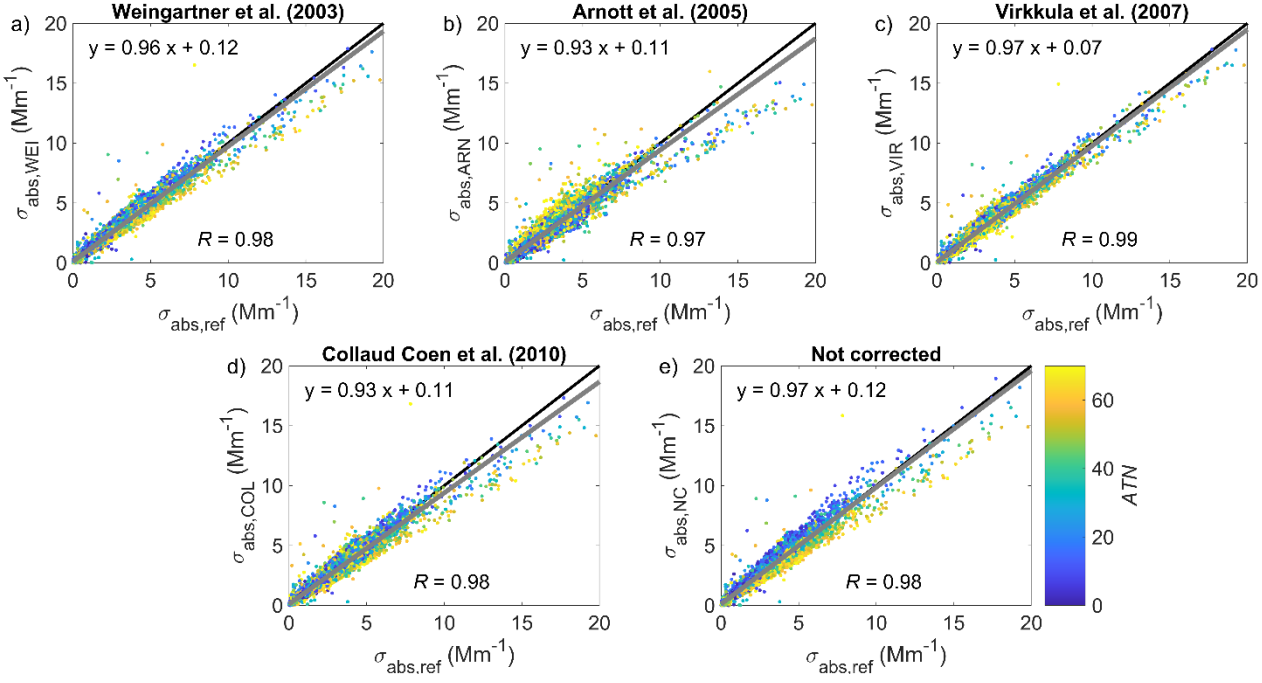

Figure 5. Comparison of the AE31 and MAAP measurements for all the different AE31 correction algorithms. The corrected AE31 data has been interpolated to the same wavelength with MAAP (637 nm). The data points are colored by the AE31 filter attenuation (*ATN*; at 660 nm). The fit to the data is presented with a grey line and the equation and the correlation coefficient are shown in the subfigures. One-to-one line is shown with black color.

https://doi.org/10.5194/amt-2020-325
Preprint. Discussion started: 8 September 2020

Atmospheric Measurement Techniques Discussions

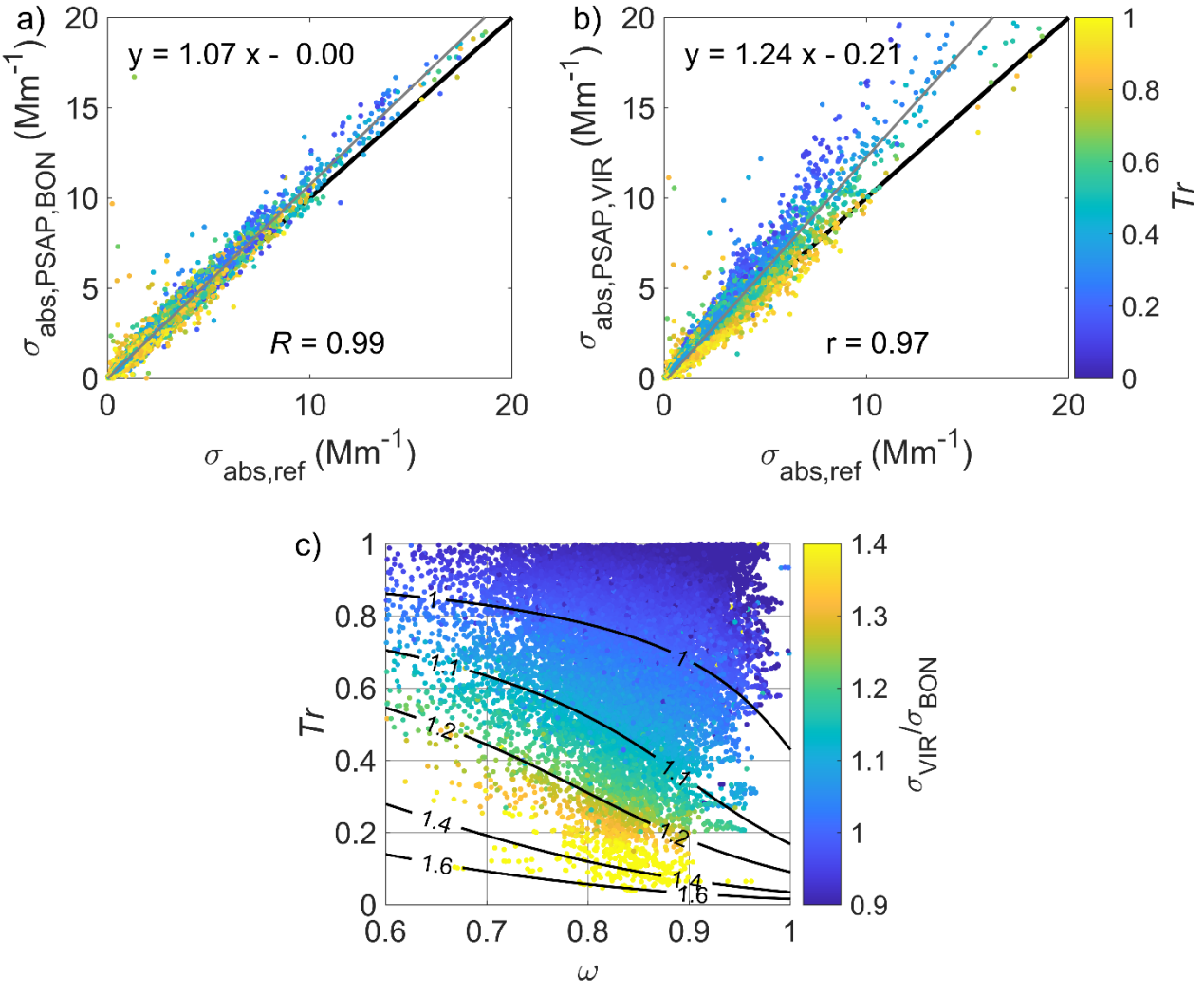

Figure 6. The a) and b) subfigures present the comparison of the PSAP and MAAP measurements for both B1999 and V2010 correction algorithms, respectively. The data points are colored be the PSAP filter transmittance (*Tr*), the fit to the data is presented with a grey line, and the equation and the correlation coefficient are shown in the subfigures. One-to-one line is shown with black color. The subfigure c) presents the relation of the PSAP derived absorption coefficients corrected with the V2010 algorithm ($\sigma_{abs,PSAP,VIR}$) and the B1999 algorithm depends on the *Tr* and single scattering albedo (ω). The contour lines show the theoretically determined $\sigma_{abs,PSAP,VIR}/\sigma_{abs,PSAP,BON}$ ratio. The ω was determined from nephelometer and MAAP measurements at 637 nm.

https://doi.org/10.5194/amt-2020-325
Preprint. Discussion started: 8 September 2020

Atmospheric Measurement Techniques Discussions

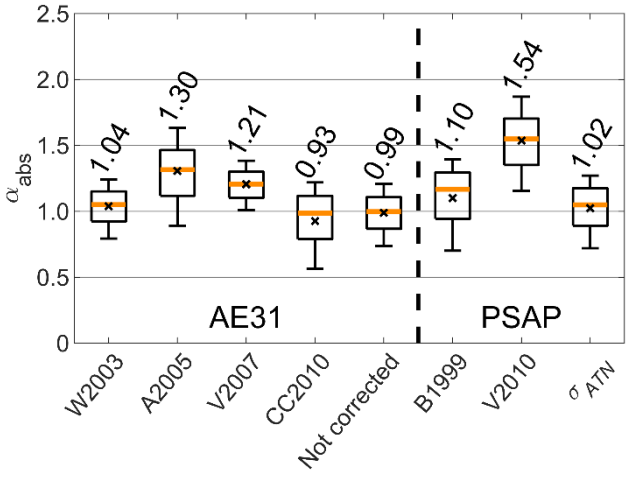

Figure 7. The absorption Ångström exponent (α_{abs}) for all the different AE31 and PSAP correction algorithms. The explanation for the boxplots is the same as in Fig. 5.

https://doi.org/10.5194/amt-2020-325
Preprint. Discussion started: 8 September 2020

Atmospheric Measurement Techniques Discussions

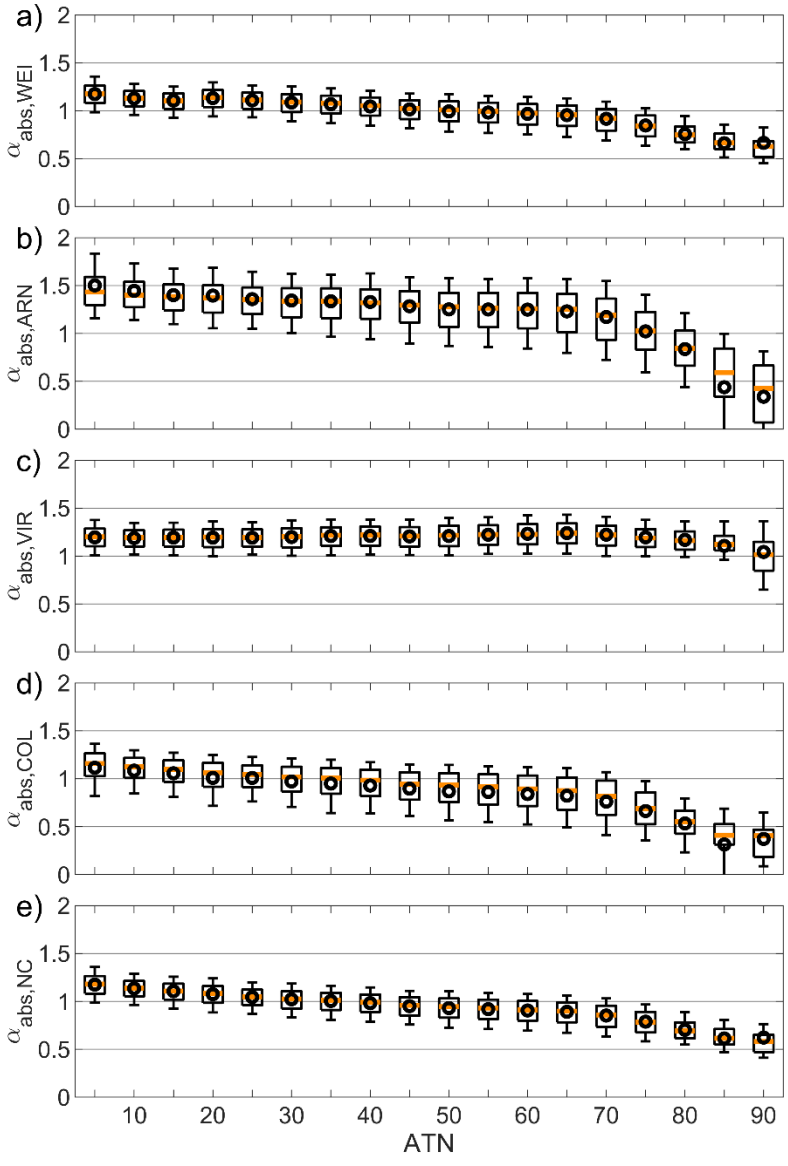

Figure 8. The dependency of the absorption Ångström exponent (α_{abs}) on the AE31 filter attenuation (*ATN*; at 660 nm) for different correction algorithms. The explanation for the boxplots is the same as in Fig. 5.

https://doi.org/10.5194/amt-2020-325
Preprint. Discussion started: 8 September 2020

Atmospheric Measurement Techniques Discussions

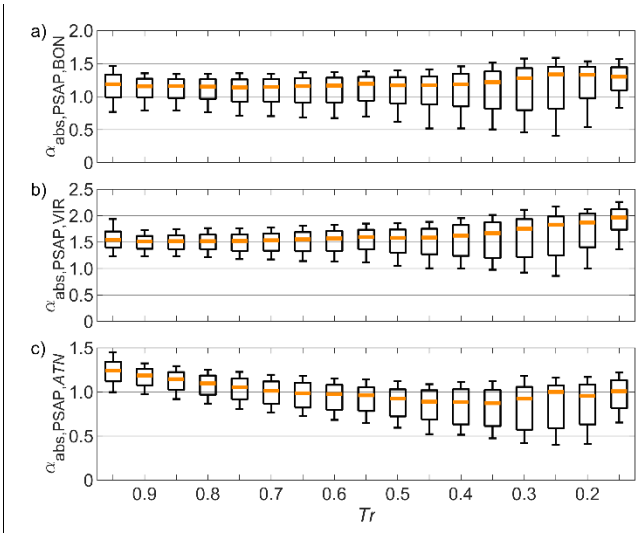

Figure 9. The dependency of the absorption Ångström exponent (α_{abs}) on the PSAP filter transmittance (*Tr*) for the a) B1999, b) V2010, and c) not corrected σ_{ATN}. The explanation for the boxplots is the same as in Fig. 5.

https://doi.org/10.5194/amt-2020-325
Preprint. Discussion started: 8 September 2020

Atmospheric Measurement Techniques Discussions

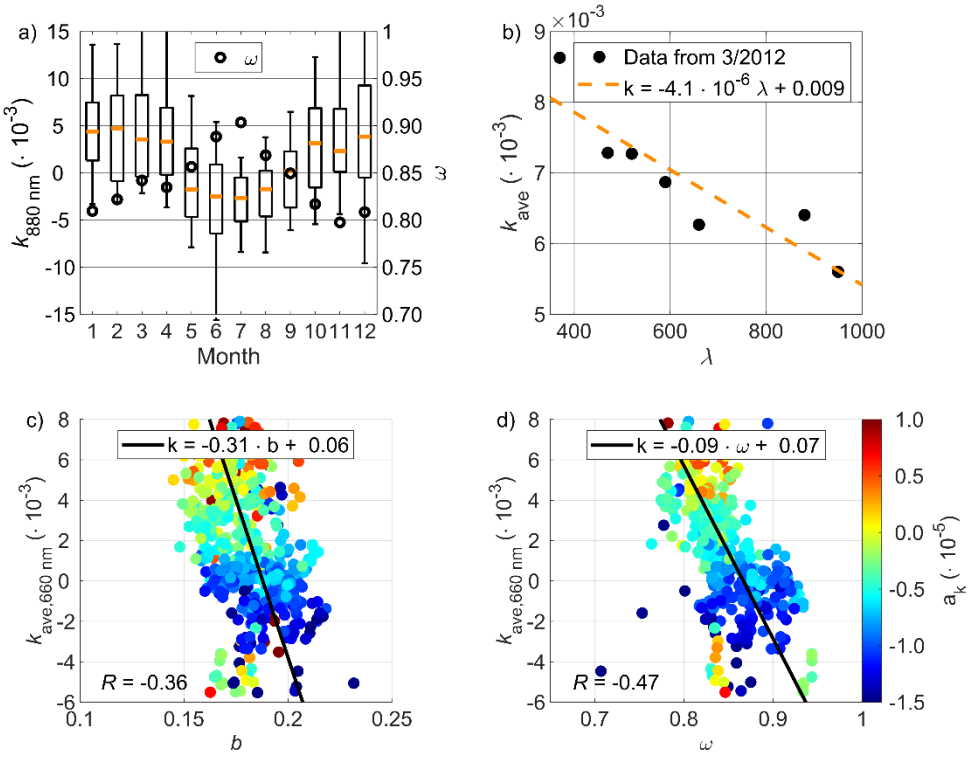

Figure 10. a) The seasonal variation of the compensation parameter (*k*). b) An example of calculating the wavelength dependency of the *k* (a_k). c) The dependency of the *k* on the backscatter fraction (*b*). The data points are coloured by a_k. d) The dependency of the *k* on the single scattering albedo (*ω*). The data points are coloured by a_k.